Statistical Analyses of Satellite Cloud Object Data from CERES. Part IV: Boundary-layer Cloud Objects During 1998 El Niño

Kuan-Man Xu[1], Takmeng Wong[1], Bruce A. Wielicki[1] and Lindsay Parker[2]

[1]NASA Langley Research Center, Hampton, VA
[2]Science Applications International Corporation, Hampton, VA

Submitted to
Journal of Climate

October 3, 2006

Corresponding author address:
Dr. Kuan-Man Xu
Climate Science Branch
NASA Langley Research Center
Mail Stop 420
Hampton, VA 23681
e-mail: Kuan-Man.Xu@nasa.gov

Abstract

Three boundary-layer cloud object types, stratus, stratocumulus and cumulus, that occurred over the Pacific Ocean during January-August 1998, are identified from the CERES (Clouds and the Earth's Radiant Energy System) single scanner footprint (SSF) data from the TRMM (Tropical Rainfall Measuring Mission) satellite. This study emphasizes the differences and similarities in the characteristics of each cloud-object type between the tropical and subtropical regions and among different size categories and among small geographic areas. Both the frequencies of occurrence and statistical distributions of cloud physical properties are analyzed.

In terms of frequencies of occurrence, stratocumulus clouds dominate the entire boundary-layer cloud population in all regions and among all size categories. Stratus clouds are more prevalent in the subtropics and near the coastal regions, while cumulus clouds are relatively prevalent over open ocean and the equatorial regions, particularly, within the small size categories. The largest size category of stratus cloud objects occurs more frequently in the subtropics than in the tropics and has much larger average size than its cumulus and stratocumulus counterparts.

Each of the three cloud object types exhibits small differences in statistical distributions of cloud optical depth, liquid water path, TOA albedo and perhaps cloud-top height, but large differences in those of cloud-top temperature and OLR between the tropics and subtropics. Differences in the sea surface temperature (SST) distributions between the tropics and subtropics influence some of the cloud macrophysical properties, but cloud microphysical properties and albedo for each cloud object type are likely determined by (local) boundary-layer dynamics and structures. Systematic variations of cloud optical depth, TOA albedo, cloud-top height, OLR and SST with cloud object sizes are pronounced for the stratocumulus and stratus types, which are related to systematic variations of the strength of inversion with cloud object sizes, produced by large-scale subsidence. The differences in cloud macrophysical properties over small regions are significantly larger than those of cloud microphysical properties and TOA albedo, suggesting a greater control of (local) large-scale dynamics and other factors on cloud object properties. When the three cloud object types are combined, the relative population among the three types is the most

important factor for determining the cloud object properties in a Pacific transect where the transition of boundary-layer cloud types takes place.

1. Introduction

It is well known that there are remarkable regional differences in cloud regimes associated with the Hadley circulation in the tropics and subtropics. Convective cloud systems are formed in the ascending regions of the Hadley circulation, i.e., deep precipitating cloud systems in the inter-tropical convergence zone (ITCZ), while boundary-layer clouds are formed predominantly in the subtropical regions associated with the descending regions of the Hadley circulation. This is related to the fact that in general, subsidence increases from the Tropics to the midlatitudes. Another important factor for the formation of boundary-layer clouds is the cold ocean water in upwelling regions, such as off the west coasts of the continents. These areas are favorable to the formation of temperature inversions. The inversion characterizes the boundary where warm and dry air produced by the subsidence overlies the boundary-layer cloud in the top portion of a well-mixed layer. The strength of the inversion and the turbulent structure of the boundary layer driven by ocean surface turbulent fluxes determine the predominant type of boundary-layer clouds. Generally speaking, stratus clouds are formed over strong subsidence regions with cold water while cumulus clouds are formed over weak subsidence regions with warm water.

The general picture of boundary-layer cloud types in relation to the Hadley circulation outlined above, however, obscures the variabilities of cloud regimes in the tropical and subtropical regions (e.g., Klein and Hartmann 1993; Weare 2000). For example, little attention has been paid to study boundary-layer clouds over the tropical open oceans where subsidence induced by deep convection (with limited spatial extent) can also form temperature inversions and produce boundary-layer clouds in the vicinities of deep convective systems (Figs. 1 and 2). These boundary-layer clouds are less persistent and less widespread than their subtropical counterparts, but they are nevertheless an important contributor to the radiative energy budget and tropical dynamics (e.g., Randall et al. 1984; Greenwald et al. 1995).

Observations of boundary-layer clouds include short-term field experiments (such as ship cruises) and long-term extensive measurements from surface weather stations and satellites. The former can provide detailed case studies and understanding of physical processes by examining

boundary-layer structures of turbulence and clouds (Albrecht et al. 1988, 1995; Stevens et al. 2003; Bretherton et al. 2004). As discussed in Xu et al. (2005; hereafter, Part I), case studies from field experiments, although they are invaluable for detailed understanding of physical processes, are unable to solve the cloud-radiative feedback problem, which requires measurements made over a wide range of temporal and spatial scales (Wielicki et al. 1995). Furthermore, these field experiments were taken place at a few geographic locations where a specific boundary-layer cloud type dominated and the variabilities of cloud types were usually small.

Satellite measurements of boundary-layer clouds are most often used to study the cloud-radiative feedback problem (Rossow and Schiffer 1991, 1999; Greenwald et al. 1995; Rozendaal et al. 1995; Hahn et al. 2001; Rozendaal and Rossow 2003; Rossow et al. 2005) because of the global coverage and the high temporal resolution. Surface weather stations also provide long-term observations of cloud amount, cloud type and precipitation, but not cloud microphysical and radiative properties (Hahn et al. 2001). The ISCCP (International Satellite Cloud Climatology Project; Schiffer and Rossow 1983) cloud statistical data provide useful information about cloud distributions by placing clouds in categories according to both their altitude and optical depth. Each cloud category is represented in terms of the cloud optical depth (τ)-cloud top pressure (P_c) pair. The frequencies of occurrence of different cloud categories are represented by the τ-P_c diagram with six τ intervals and seven P_c intervals (Rossow and Schiffer 1991, 1999). The low-level clouds, which correspond to pressures greater than 680 hPa, are represented by three τ intervals that were named "cumulus" (τ from 0.1 to 3.6) "stratocumulus" (τ from 3.6 to 23) and "stratus" (τ greater than 23). These τ ranges correspond well with climatological values of these cloud types, but are not consistent with the τ ranges of these cloud types inferred from instantaneous observations by ground-based observers (Hahn et al. 2001). Hahn et al. (2001) found that the distribution patterns for the individual low cloud types occurring alone overlap to such an extent that it is impossible to distinguish these cloud types from each other on the basis of τ-P_c

values alone. That is, the cloud categories in the τ-P_c diagram do not have a one-to-one correspondence with cloud types as seen by ground-based observers.

In order to separate particular cloud processes from numerical model simulations and satellite data, compositing methods must be used to define various cloud regimes that exhibit unique processes based upon synoptic-scale conditions (Lau and Crane 1995, 1997; Tselioudis et al. 2000; Tselioudis and Rossow 2006) or statistical cloud classifications (Jakob et al. 2005; Rossow et al. 2005; Xu et al. 2005). Examples of the statistical cloud classifications include the cluster analysis of the ISCCP cloud statistical data by Jakob et al. (2005) and Rossow et al. (2005) and the cloud object analysis of cloud system types by Xu et al. (2005). The cluster analysis uses the ISCCP cloud category frequency data on large grid boxes to deduce 4-5 different cloud regimes. The method is able to deduce a boundary-layer cloud regime even in convectively dominant regions (Jakob et al. 2005).

The cloud object analysis, on the other hand, identifies a cloud object as a contiguous patch of cloudy footprints that possess similar cloud physical properties. The shape and size of a cloud object are determined by the satellite footprint data and by the selection criteria for a given cloud-system type. No arbitrary grid of the Earth is used in the analysis of satellite data, as opposed to the Eulerian approach used in the monthly-averaged satellite data. Because the selection criteria used in the cloud object analysis are based upon cloud physical properties, the cloud types determined from this analysis closely resemble those seen by ground-based observers, compared to the ISCCP classification. As discussed in Part I and in section 2 of the present study, cloud fraction of satellite footprints is used to distinguish boundary-layer stratus, stratocumulus and cumulus cloud types. Cumulus clouds have a smaller cloud fraction than that of stratocumulus and stratus clouds while stratus clouds are overcast.

A broader application of this cloud-object approach is to integrate observational data analysis and high-resolution modeling to improve the understanding of cloud feedbacks, as discussed in Xu et al. (2006; hereafter Part II). This includes two major steps. First, satellite data are analyzed to generate large ensembles of cloud objects and they are combined to produce statistically

robust cloud-physical characteristics to reach climate accuracy (Ohring et al. 2005) for different cloud-system types. Second, the atmospheric state is matched to each cloud object in space and in time in such a way to allow for stratification of observed cloud objects according to some independent measures of the atmospheric states. This is needed to derive the partial derivatives of cloud properties versus atmospheric states, or individual components of cloud feedbacks (Schlesinger 1985).

Part I of this series outlined the details of the cloud object data analysis methodology and presented some preliminary results from the analysis of the statistical properties of tropical deep convective and three boundary-layer cloud objects associated with the strong 1997/98 El Niño in March 1998 and the weak 2000 La Niña in March 2000, based upon the TRMM/CERES [Tropical Rainfall Measuring Mission/Clouds and the Earth's Radiant Energy System; Wielicki et al. (1996)] footprint data. Part II presented results for deep convective cloud object for the period of January-August 1998 while Part III presented cloud-resolving model simulation results for deep convective cloud objects (Luo et al. 2006). In the present study, both the frequencies of occurrence and statistical properties of boundary-layer cloud objects will be analyzed for the period of January-August 1998. The objectives of this study are threefold: 1) to find similarities and differences between the tropical and subtropical boundary-layer cloud objects, 2) to find similarities and differences among three size categories of cloud objects and 3) to examine the variabilities of boundary-layer cloud objects in small geographic regions. The overarching goal is to identify the physical processes that are most likely related to the large variations in cloud microphysical, macrophysical and radiative properties in the analyses. The present study extends the analysis of Part I to a longer period in more detail. The differences in cloud-object characteristics among the three types were examined in Part I and therefore will only be briefly discussed in this study.

The rest of the paper is organized as follows. Data and methodology are briefly outlined in section 2. Results for different aspects of the analysis are presented in sections 3-6. Summary and discussion are given in section 7.

2. Data and methodology

2a. Footprint data for generating cloud objects

The details of the cloud object methodology and the data used in generating the cloud object data product are presented in Part I. Briefly, the basic data from which the cloud object data are produced are a level-2 CERES Single Scanner Footprint (SSF) TOA/Surface Fluxes and Clouds data product (Wielicki et al. 1996), which includes cloud optical, microphysical (e.g., liquid water path) and macrophysical (e.g., cloud top height and temperature) properties derived using multispectral data from the Visible/Infrared Scanner (VIRS), and broadband top-of-the-atmosphere reflected shortwave (SW), emitted longwave (LW) fluxes from the CERES scanner. Only the footprint data corresponding to viewing zenith angle (VZA) less than 48° and in regions between 38° S and 38° N are used due to the restricted VZA of the VIRS instrument.

The CERES broadband radiative fluxes are produced using the new generation of Angular Distribution Models (ADMs) derived from TRMM (Tropical Rainfall Measuring Mission) CERES broadband radiance observations (Loeb et al. 2003). The cloud micro- and macro-physical properties are retrieved from the higher-resolution VIRS cloud imager measurement and supplemented with sounding information from a data assimilation system. These cloud imager-based data are energy-weighted averaged over the larger CERES footprints. Details of the retrieval methods are described in the CERES algorithm theoretical basis document (Minnis et al. 1997). Uncertainties in the retrieved parameters will be described in section 2c.

2b. Cloud object methodology

A cloud object is defined as a contiguous patch of cloudy regions composed of individual satellite footprints that meet a set of physically-based selection criteria. A “region-growing” strategy based on imager-derived cloud properties is used to identify cloud objects within a single satellite swath (Wielicki and Welch 1986). For all CERES footprints in a TRMM satellite orbit swath, each CERES footprint that meets the selection criteria is marked as specific cloud type. These “seed points” are grown using the Wielicki-Welch algorithm. Only footprints that are adja-

cent and that meet the selection criteria of a single cloud type can be joined in a cloud object. By adjacent, we mean CERES footprints that are next to each other either along the scanning direction or perpendicular to it. Cloud objects are uniquely determined when they share no adjacent footprints. Any cloud object that grows to an equivalent diameter (of a circle) of greater than 75 km (43 footprints) is saved in the cloud object database (http://cloud-object.larc.nasa.gov/), so are the atmospheric state data that are matched in time and in space with the cloud object. We choose an average footprint area of 10 x 10 km^2 to calculate the equivalent diameter, which can cause one-sigma error in cloud object diameter of roughly 20%. The procedure for matching the cloud object with atmospheric state data was given in Part II.

The selection criteria for boundary-layer cloud-object types, as mentioned in section 1, are composed of both cloud-top height and cloud fraction (Table 1). The cloud-top height must be less than 3 km, which is sufficiently high for such clouds without an overlapping high cloud above. The cloud fraction of the footprint must be between 99-100% to be stratus, 40-99% to be stratocumulus and 10-40% to be cumulus. After a cloud object is identified, each footprint is checked to screen out any ice cloud footprint so that only water clouds are included in the data. The threshold of 40% for separating cumulus and stratocumulus clouds is arbitrary, but the lower limit of 10% for cumulus clouds is designed to eliminate uncertainties associated with satellite imager measurements. The selection criteria used in this study are, as discussed in section 1, adequate for categorizing the three boundary-layer cloud types seen by ground-based observers, compared to the classification by the ISCCP (Rossow and Schiffer 1991, 1999). However, additional information such as imager-pixel variabilities would be needed to more rigorously categorize these cloud types seen by ground-based observers. This step was not taken because the present study is not aimed at comparing satellite data with ground-based observations.

2c. Uncertainties in the measurements

As in any type of observations, there are uncertainties in the measured/retrieved parameters examined in this study. It is challenging to assign rigorous uncertainty estimates to remotely-

sensed products because direct validation measurements are scarce. The uncertainty estimates to be provided below are based either upon the understanding of the instrument's measurement (Loeb et al. 2006a, b) or upon limited amount of direct validation measurements from ground-based instruments (Dong et al. 2002; Garreaud et al. 2001). In the latter case, the uncertainties also include those of ground-based instruments and space/time matching of surface to satellite data. The uncertainty values are listed in Table 2, along with bin intervals of histograms.

For the top-of-the-atmosphere albedo and LW radiative fluxes, the systematic biases are less than 0.5% while the random errors are 1-2% for LW fluxes and 2-3% for albedo, respectively (Loeb et al. 2006a, b). These are mainly contributed by calibration and angle sampling errors. Uncertainty estimates of cloud optical depth, liquid water path and droplet effective radius were based upon comparisons with retrievals of the same quantities from surface-based instruments at the Atmospheric Radiation Measurement site in Oklahoma (Dong et al. 2002). The VIRS daytime retrievals agreed excellently with surface and aircraft retrievals for stratus clouds (Table 2), i.e., cloud optical depth: -1.5 ± 6.2 ; LWP: -18 ± 41 g m^{-2}; effective radius: 0.7 ± 1.8 μm. It is expected that the errors for broken clouds are, however, larger for these quantities. Cloud temperature is the mean radiating temperature within a few 100 m of the top, with errors of 0.9 ± 2.1 K, compared to that determined from surface soundings [The random error is only 1 K for oceanic clouds; Garreaud et al. (2001)]. Cloud-top height is obtained from the difference between sea surface temperature (SST) and cloud-top temperature using a constant lapse rate of 7.1 K km^{-1}. The errors associated with cloud-top height retrieval are 0.2 ± 0.3 km. The constant value of lapse rate may be a source of errors when the heights of cloud objects among different regions are compared.

These various types of uncertainties are somewhat detrimental to understanding the relationships of cloud and atmospheric dynamics. This is especially true for any small set of cloud observations such as might be examined in a short field experiment. The current study attempts to partially overcome these uncertainties by focusing on relationships derived from frequency distributions of very large samples of both clouds and atmospheric state. As shown later, the ranges of

cloud and radiative flux variations in the frequency distributions far exceed the instantaneous uncertainties, as well as the systematic biases. Tests adding such errors to the distributions in Part II concluded that the statistical results are robust despite these errors.

2d. Period of analysis and geographic distribution of cloud objects

Eight months (January-August 1998) of the TRMM CERES data are analyzed in this study. These eight months correspond to the nearly peak and dissipative phases of the 1997/1998 El Niño. The TRMM orbits span the regions between 38 °S and 38 °N. Because of the TRMM inclined orbit (see Fig. 10 in Wielicki et al. 1996), same cloud objects observed to the south of 30 °S and the north of 30 °N are identified several times a day. Exclusion of these cloud objects allows summary histograms of cloud-physical characteristics be nearly evenly contributed by cloud objects observed in different latitudinal bands. This eliminates one third of the cloud object population identified from this data period.

The accumulated numbers of cloud objects in 5° x 5° areas in the Pacific are shown in Figs. 1 and 2 for all cloud objects with equivalent diameters greater than 150 km and 75 km, respectively. The total number of cloud objects shown in Fig. 1 is 9,161. There are an additional 39,619 cloud objects shown in Fig. 2 that have equivalent diameters between 75 and 150 km. The corresponding total footprint numbers are 5.305 million and 8.362 million for the cloud objects shown in Figs. 1 and 2. This indicates that the large-size cloud objects dominate the total footprint numbers, which is the reason for showing Fig. 1 separately.

The geographic distributions of cloud objects have distinct features among the three cloud-object types. First, there are three maximum frequency centers in the subtropical regions except for the large-size cumulus population (Fig. 1): one in the northern hemisphere off the coast of California, two in the southern hemisphere (i.e., central Pacific and off the South America coast). The central Pacific maximum and the westward extension of the maximum center in the northern hemisphere are related to the eastward migration of the Walker circulation during the El Niño period. Second, the stratus population is located further eastwards than the stratocumulus

and cumulus population and the stratocumulus population is located further eastwards than the cumulus population. Third, there are relatively few stratus cloud objects and relatively more cumulus cloud objects in the equatorial region, particularly for the large size population (Fig. 1). Both the second and third features are linked to both the longitudinal change in the strength of large-scale subsidence and the SST distribution.

In the analyses presented below, both frequencies of occurrence and statistical properties for cloud objects sorted by cloud system types and their sizes are examined, as in Part II. These cloud objects are further sorted by geographic locations of various sizes because of the much wider ranges of SST variations associated with these cloud objects than those of tropical convective cloud objects examined in Part II. Unlike Part II, the matched atmospheric state parameters, such as the surface divergence and low-level stability, will not be presented because of large uncertainties in the assimilated meteorological data. Further discussion will be given in section 7

3. Tropical vs subtropical boundary-layer clouds

3a. Frequency of occurrence

In the following, comparisons of cloud object population focus upon the relative frequency between the two regions or two size categories, instead of their total numbers of occurrence. The total numbers of boundary-layer cloud objects identified over the tropical and subtropical Pacific regions from the CERES SSF data are listed in "All sizes" columns of Table 3. The relative frequencies are shown according to the range of their equivalent diameters. Four size categories are considered. They are labeled as sizes S1, S2, S3 and S4, corresponding to the equivalent diameter ranges from 75 - 100 km (S1), 100 - 150 km (S2), 150 - 300 km (S3) and greater than 300 km (S4), respectively. The staggered size intervals were chosen because of the well-known exponential decrease of cloud population with size. As in Rossow et al. (2005), we define the region between 15 °S and 15 °N as the tropics and that of 15 °S to 30 °S and 15 °N to 30 °N as the subtropics, whereas Wielicki et al. (2002) chose the region between 20 °S and 20 °N

to obtain tropical mean TOA fluxes. The present definition of the tropics may be too narrow to include the seasonal migration of the ITCZ for all longitudes.

It is apparent from Table 3 that the smallest (S1 size) cloud objects appear much more frequently than the larger cloud objects in both the subtropics and tropics for all three cloud object types (47.8%-50.1%) although the interval of the equivalent diameter range (25 km) for this size category is considerably smaller than that of the other size categories. For example, the S1 size category has 61.7% of a total of 12,026 cumulus cloud objects. The stratocumulus type, which dominates the overall cloud-object population, also has a higher percentage (46.2-47.8%) of the smallest-size cloud objects than the stratus type (38.0-40.5%).

The relative frequencies among the four size categories of any cloud object type are nearly identical (within 2.5%) between the tropical and subtropical regions except for a slightly higher percentage (by 5.7%) of the S4 stratus cloud objects in the subtropics. The relative frequencies are higher for S2, S3 and S4 categories in the subtropics than in the tropics. The accumulated total cloud-object number is also higher in the subtropics, in particular, by ~50% for stratus cloud objects. These results are related to the differences in the strength of the large-scale subsidence and the temperature inversions at the top of the boundary layer between the two regions. Weaker subsidence and weaker inversions favor cumulus cloud objects but stronger subsidence and stronger inversions favor stratus cloud objects. The persistence of stratus and stratocumulus cloud types in several subtropical areas is another reason for the difference (Figs. 1 and 2).

The total footprint numbers in a cloud object category can provide additional information on the relative importance of a specific cloud object category in the total population and the difference of the same cloud object category between the tropical and subtropical regions. The total footprint number multiplied by the average footprint size (10x10 km^2) corresponds to the total area coverage. Table 4 shows that the total footprint numbers for the all-size category in the subtropics are higher by 15% for cumulus, 48% for stratocumulus and 187% for stratus cloud objects than their tropical counterparts while the numbers of cloud objects in the subtropics are only higher by 11%, 19% and 53% for these three types of cloud objects, respectively (Table 3). This

result is related to the dominant contributions by the S4 size category in the subtropics. For example, the subtropical S4 category contributes to the total footprint numbers nearly twice as much as in the tropics for both stratocumulus (32.3% vs. 16.3%) and stratus (68.4% vs. 37.1%) cloud objects. This can be further related to the larger average footprint numbers of subtropical stratocumulus and stratus cloud objects, as shown in Table 5, because they are more persistent over a few areas (Fig. 1). On the other hand, cumulus cloud objects have relatively small total footprint numbers (Table 4), compared to the stratus or stratocumulus cloud object types because they have fewer large size cloud objects (Table 3) and their averaged footprint numbers are smaller than the other two types (not shown). Consequently, the smallest size category is the largest contributor to the total footprint numbers for cumulus cloud objects (Table 4).

3b. Statistical characteristics of cloud properties

As in Parts I and II of this series, summary histograms of cloud physical properties are examined to illustrate the statistical differences between the tropical and subtropical boundary-layer cloud objects in this section. There are significant differences in all statistical properties among the three cloud-object types and between the tropics and subtropics (Figs. 3-5). All cloud objects with equivalent diameters between 75 and 300 km are included in producing the summary histograms using between 0.5 and 1.7 million footprints. In Part I, similar statistical differences among the three cloud object types were found in the summary histograms of several parameters over monthly periods for smaller geographic regions. They are consistent with past (Wielicki and Parker 1992; Barker et al. 1996; Barker and Wielicki 1997) and recent results (Szczodrak et al., 2001; Wood and Hartmann 2005). So, these differences in statistical properties among the cloud-object types will not be discussed in detail. Please refer to Part I for further discussion. In the following, the differences between the tropics and subtropics for each of these cloud object types will be discussed in detail, so will be the relative changes in the differences among the three cloud object types. Some of the differences between the two regions to be discussed below are so large that there is no need to perform a statistical significance test as in Parts I and II using the bootstrap method proposed by Xu (2006). This method will be used in section 4.

For the shallow cumulus cloud objects, the differences in the summary histograms of all cloud physical properties, except for cloud optical depth, liquid water path (not shown) and albedo, between the tropics and subtropics are pronounced (Fig. 3). The SST distributions are rather different (Fig. 3a), with modes at 301.8 K for the tropics and 299.8 K for the subtropics, respectively. The subtropical SST distribution is much broader, with SSTs as low as 290 K, compared to a minimum SST of 295 K for the tropical distribution, although the maximum ranges are similar, at 304 K. The large SST differences between the two regions have the most impact on the cloud macrophysical properties, particularly, by shifting the modes of the OLR and cloud-top temperature distributions and broadening the subtropical distributions of cloud-top height and temperature. For example, the modes of the cloud-top temperature distributions (Fig. 3e) differ by 2 K between the two regions while those of OLR distributions (Fig. 3c) differ by 6 W m^{-2}.

The small differences in the cloud optical depth and albedo distributions between the two regions (Figs. 3b, f) are perhaps related to the lack of differences in cloud thickness and cloud fraction, as well as large biases in the measurements. The lower bound of cloud top heights for both regions (Fig. 3d), compared to the other two cloud-object types shown later (Figs. 4d and 5d), is likely an artifact of the subpixel effect of this cloud-object type. The retrieval algorithm can underestimate the actual heights of cumuli because their physical size can be smaller than the individual imager footprint (~ 2x2 km^2).

For the stratocumulus cloud objects, the differences in the cloud macrophysical properties between the tropics and subtropics are also pronounced although there is no discernible difference in the liquid water path (not shown), cloud optical depth (Fig. 4f) and albedo (Fig. 4b) distributions. The mode separation in the cloud-top temperature distributions (Fig. 4e) between the two regions is 4 K. The modes of cloud top heights are located around 1.2 km, with more power of slightly higher cloud tops in the subtropics (Fig. 4d). Slightly more power of lower OLRs also appears in the subtropics (Fig. 4c). All of these results are related to the large differences in the SST distributions between the two regions (Fig. 4a).

The differences in the stratus cloud objects between the two regions are also more significant in the macrophysical properties than in the microphysical properties and TOA albedo (Fig. 5). The SST distribution is more normally distributed than its cumulus and stratocumulus counterparts. This means that stratus clouds prefer more cold oceanic areas, compared to the other two cloud types (see Figs. 1 and 2). The mode of the tropical SST distribution shifts to a lower value. The modes of cloud-top temperature shift to lower values (283 K for the subtropics and 287 K for the tropics), so do the modes of the OLR distributions (273 W m^{-2} for the subtropics and 277 W m^{-2} for the tropics). These results are related to higher cloud fractions of stratus footprints and larger differences in the cloud-top height distributions between the two regions (Fig. 5d). In the subtropics, there are more occurrences of stratus clouds with high tops, compared to their tropical counterpart. This suggests that there are larger differences in boundary-layer structures and stratification for this type of clouds between the two regions although the constant lapse rate used in diagnosing cloud-top height (Garreaud et al. 2001) may not be ruled out as a reason for the differences. The differences in the stratification, particularly, the inversion strength, are highly related to those in the boundary-layer turbulence and cloud structures.

The cloud optical depth shows almost no difference between the tropics and subtropics (Fig. 5f). However, the TOA albedo distributions are slightly different, with the modes differing by 0.02 (Fig. 5b). That is, the albedo is slightly higher for the subtropical stratus cloud objects. A likely explanation is that there is a higher proportion of large-size cloud objects in the subtropics than in the tropics. The large-size cloud objects, as shown in section 4, tend to be brighter, which are related to the increasing strength of large-scale dynamics with the horizontal dimension.

In summary, each of the three cloud object types exhibits small differences in cloud optical depth, liquid water path, TOA albedo and perhaps cloud-top height, but large differences in cloud-top temperature and OLR between the tropics and subtropics. The latter two properties are tightly related to the differences in the SST distributions between the tropics and subtropics. It should be pointed out that these differences between the tropics and subtropics are smaller than those among the cloud object types shown in Figs. 3-5 and Part I. These results suggest that SST

distributions strongly influence cloud macrophysical properties, but only weakly influence cloud microphysical properties and albedo for each cloud object type. The latter distributions are robustly determined by distinct boundary-layer dynamics and structures of each cloud object type.

4. Variation of subtropical cloud objects with size

Part I presented statistical distributions of the S2 size category in the southeast Pacific region for two short periods. In this section, variations of cloud object characteristics with size will be discussed. For simplicity, only those of subtropical cloud objects will be examined because the total footprint number for each size category of cloud objects is larger in the subtropics than in the tropics (Table 4). For stratocumulus and stratus cloud objects, S2, S3 and S4 size categories are compared. S1, S2 and S3 size categories are compared for cumulus cloud objects because there are a few cloud objects in the S4 size category (Table 3). Because differences among size categories are small for some histograms, it is necessary to perform statistical significance tests based on the bootstrap method. The detailed procedure for this test was presented in Xu (2006). Table 6 shows the statistical significance level (p) or p-value for testing between a pair of size categories of a cloud object type. The threshold p-value is customarily chosen to be 0.05. That is, there is 95% confidence that the two pdfs are significantly different. When the p-value is less than 0.05, there is more than 95% confidence that the two summary histograms are not formed from a statistically similar cloud-object population. It should be cautioned that there are, as discussed in section 2c, large uncertainties in remotely sensed cloud parameters, especially those of broken clouds, so that some apparently significant differences may be in fact insignificant. Therefore, a smaller threshold p-value such as 0.01 is recommended.

For the cumulus cloud objects, the differences in the summary histograms among the three size categories are small for all parameters except for the following cases. The TOA albedo of the S3 size category and cloud-top height of the S1 size category are different from those of the other size categories (Fig. 6 and Table 6). The slight shift of OLR towards higher values for the S3 size category is related to the changes in cloud-top height and temperature. That is, it is related to

the increase of the probability densities for lower cloud-top heights (< 1 km) and higher cloud-top temperatures (> 290 K). The TOA albedo for the S3 size category is also higher than the other size categories although the cloud optical depth does not show any difference among the three size categories. This is likely related to the variation of solar zenith angle with latitude.

For the stratocumulus cloud objects, the distributions of all cloud physical properties are different among the three size categories (Fig. 7 and Table 6), except for OLR between S3 and S4 size categories and SST between S2 and S3 size categories. The SST distributions shift to lower SST values as the cloud object size increases. The modes of the distribution between S3 and S4 size categories differ by 1.5 K, at 297.3 K for S3 and 295.8 K for S4, respectively. The SST distribution for the S4 size category is smoother and more Gaussian-like, which is statistically different from that of the S2 and S3 size categories (Table 6). Unlike those in the shallow cumulus cloud objects (Fig. 6), variations of all cloud physical properties with size are pronounced and systematic (Fig. 7). That is, the larger cloud objects have higher TOA albedos and higher cloud optical depths, similar to variations of tropical deep convective cloud objects with size discussed in Part II. However, the larger stratocumulus cloud objects have lower cloud-top heights, higher OLRs and lower SSTs, opposite to variations of tropical deep convective cloud objects with size. As explained later, these variations of cloud macrophysical properties with size are influenced by the SST distributions. Those of cloud optical depth and TOA albedo may be related to the differences in large-scale dynamics among the size categories, which is the explanation given for tropical deep convective cloud objects in Part II.

The differences in cloud-top height of the stratocumulus type are tied to those in the SST distributions. That is, the lower the SST is, the lower cloud-top height is, due to a lower boundary-layer height. However, the cloud-top temperature is lower for the S4 size category (Fig. 7e) despite of its lower SST, compared to S2 and S3 size categories. To have lower cloud-top height and temperature and lower SST simultaneously, the environments of these cloud objects must be located further away from the Equator, for example, in the stratocumulus dominated regions near midlatitudes. These long-lasting and well-organized stratocumulus cloud systems are more

dynamically driven, which means that turbulence-scale circulations are stronger. This may explain why LWP, optical depth and droplet radius are higher for the S4 size category while the OLR distributions are more strictly tied to those of cloud-top heights rather than cloud-top temperature (Fig. 7b). That is, the OLR is also strongly influenced by the amount of water vapor in the clear sky and above the cloud top.

For the stratus cloud object type, the SST distributions are rather similar to those of the stratocumulus type except that the mode of the SST distribution shifts to a lower value (from a mode value of 295.8 K for stratocumulus to 294.3 K for stratus) for the S4 size category (Fig. 8a). This suggests that these large-size cloud objects are located further away from the Equator or closer to the cold-water coastal regions (Fig. 1), compared to the large-size stratocumulus cloud objects. This characteristic of cloud objects can impact other properties of cloud objects. Another difference between the stratocumulus and stratus types is that the SST distribution for the S4 size category is also more significantly different from that of either the S2 or S3 category (Fig. 8a).

The differences among the size categories for the stratus cloud physical properties shown in Fig. 8 are rather similar to those of stratocumulus shown in Fig. 7 but with greater magnitudes in the differences for all parameters except for OLR between the S2 and S3 size categories and cloud-top temperature among the three size categories. For example, the modes of cloud optical depth and TOA albedo distributions move to larger values as the size of cloud objects increases. Both distributions are more negatively skewed for the larger size cloud objects. The cloud-top height distributions show a more systematic decrease as the size of cloud object increases. The explanation for these results is the same as that given earlier for the stratocumulus cloud type. That is, the differences in large-scale dynamics play an important role. The physical thickness of stratus clouds in the lower SST areas may not be much lower, due to simultaneous decreases of both cloud top and bottom heights, than those in the higher SST areas. The stronger large-scale subsidence in the colder SST area increases the optical thickness and the TOA albedo. The OLR, on the other hand, slightly increases due to a decrease of cloud-top height and a possibly larger difference in the amount of water vapor above the cloud top.

In summary, there are significant dependencies of nearly all cloud object properties on the horizontal sizes of cloud objects. Systematic variations of cloud optical depth, TOA albedo, cloud-top height and OLR and SST with cloud object sizes are particularly pronounced for the stratocumulus and stratus types. These results can be explained by the systematic variations of large-scale dynamics with cloud object sizes, particularly, the strength of inversion produced by the large-scale subsidence. The differences in cumulus cloud objects among the size categories are less systematic, due to weaker inversions associated with cumulus cloud objects and due perhaps to larger uncertainties in remotely-sensed measurements of broken clouds than those of contiguous clouds.

5. Differences among three eastern Pacific regions

Three boundary-layer cloud dominating regions in the eastern Pacific (Fig. 9a), which are much smaller than the two regions examined in Part I, are selected to further understand the linkage of physical processes with cloud physical properties and the frequency of occurrence. These three regions are located in the eastern equatorial Pacific (EEP; 82-120 °W; 3 °S-7 °N), southern subtropical Pacific (SSP; 82-105 °W; 5-23 °S) and northern subtropical Pacific (NSP; 120-140 °W; 15-35 °N). According to the definition given in section 3, the EEP region is located in the tropics while the NSP region is located in the subtropics. The SSP region is located partly in the tropics and partly in the subtropics. The numbers of cloud objects for the S2, S3 and S4 size categories are listed in Table 7.

Even for relatively small regions in the eastern Pacific, stratocumulus type still dominates the boundary-layer cloud populations (Table 7), which is more than 55% of the total boundary-layer cloud population. The cumulus population is less than 10% (7.1% - 9.6%) of the total in all three regions. The stratus population varies greatly from one region to another, i.e., 28.4%, 33.9% and 37.4% for the EEP, SSP and NSP regions, respectively. The larger proportion of stratus population in NSP is related to the strengthening of the Hadley circulation in the Northern Hemisphere during El Niño (Cess et al. 2001).

The proportion of different size categories in the three regions (Table 7) is different from that of either subtropical or tropical regions discussed in section 3 (Table 3). The EEP region has higher percentages of the S2 size of cumulus (89% of the sum of S2, S3 and S4 categories) and stratocumulus (70%) types than those (80% and 65%) in the tropical region. There are comparable proportions of different size categories of cumulus and stratocumulus types between the NSP and SSP regions, but the NSP region (36%) has a much higher percentage of the S4 size category of the stratus type than in the SSP region (20%). In both regions, the largest size category of stratocumulus and stratus types has a higher frequency of occurrence than that of the subtropical region because these regions are preferable locations of these cloud types (Fig. 1).

Because of the large number of stratocumulus cloud population shown in Table 7, summary histograms for this cloud object type are shown for these three regions (Fig. 10). The differences in all cloud physical properties among the three regions are much greater than those between the tropics and subtropics (Fig. 4) or among the size categories (Fig. 7). This is because of the small areas of these regions where (local) large-scale dynamics and boundary-layer structures differ greatly. Other factors such as the aerosol concentration and oceanic upwelling may play larger roles in determining the cloud physical properties, compared to a large region covering the entire tropics or subtropics of the Pacific. With this in mind, the results are discussed below.

The SST is narrowly distributed around 302 K in EEP, widely distributed in NSP and nearly normally distributed in SSP. SSP is much warmer than in NSP (Fig. 10a), due to its equatorward location and the influence of the warm ocean water during El Niño. Despite these large differences in the SST distributions, cloud optical depth and TOA albedo are nearly identical between NSP and SSP (Figs. 10c, h). This result is related to the fact that the proportion of different size categories of cloud objects is nearly identical between the two regions (Table 7). The liquid water path and droplet radius distribution in NSP is much closer to that in SSP than in EEP (Figs. 10f, g). The equatorial stratocumulus is optically thinner with less liquid water and smaller droplets. This characteristic is present in the comparison between the tropics and subtropics, but with smaller magnitudes of differences (Fig. 4). The higher proportions of smaller size cloud

objects in EEP (Table 7) likely contribute to these differences because of the systematic variations of large-scale dynamics with cloud object size discussed in section 4.

Cloud macrophysical properties and OLR follow more closely to the SST distributions. In particular, the SST distributions have the greatest impact on cloud-top temperature and OLR, as discussed in the previous sections. The cloud-top height distributions show more similarities between EEP and NSP than between SSP and NSP. The SSP clouds have a narrower range of top heights. These differences among the three regions suggest that (local) large-scale dynamics and other local factors such as aerosol concentration (as seen from droplet radius shown in Fig. 10g) become more dominating in determining the cloud macrophysical properties. The differences in cloud microphysical properties and albedo are, however, modulated by the changes of the proportion of different size categories of a cloud object type.

6. Transition of cloud object types along a Pacific transect

Another small region to be examined in this study is the Pacific transect (Fig. 9b). This region is defined by the GCSS (GEWEX Cloud System Study, where GEWEX stands for Global Energy and Water-cycle Experiment) model intercomparison project (Siebesma et al. 2004) and encompasses an area from the California coast (125 °W, 35 °N) to the equator (173 °W, 1 °S). This transect is used to examine the transition from subtropical boundary-layer clouds to tropical deep convection. The numbers of all boundary-layer cloud objects whose centers located within one of seven 5 °x 5 ° grids along the transect are shown in Table 8.

Stratocumulus clouds dominate the total boundary-layer cloud-object population in all seven grids, which are the smallest geographic areas examined in this study. Both the stratocumulus and all cloud-object type populations generally decrease away from the California coast except for Grid 2 (Table 8). Stratus clouds are more prevalent near the coastal regions while cumulus clouds are relatively prevalent over open oceans. Grid 1 has the highest stratocumulus and cumulus populations but their average sizes (271 and 145 footprints) are much smaller than that of stratus cloud objects (1127 footprints), due perhaps to large variations of synoptic condi-

tions near the coast. Grid 2 has the lowest cumulus population while its stratocumulus population is also relatively low. Its average stratus cloud object has 2316 footprints, compared to 341 footprints for stratocumulus and 141 for cumulus. Thus, the presence of these large-size stratus cloud objects in this grid dominates the overall characteristics of cloud physical properties to be shown below. As expected, the total footprint number of all cloud object types rapidly decreases as the grid moves away from the stratocumulus dominating region that is an area corresponding to Grids 1, 2 and 3.

The transition from stratus-dominated to cumulus-dominated regimes across this Pacific transect are best represented by the cloud microphysical properties and TOA albedo (Figs. 11c, f and h). In Grids 1 and 2, histograms of these parameters are much closer to the normal distributions than other grids and there are higher probability densities in the high ranges of TOA albedo, LWP and τ. Both characteristics are typically observed only for the stratus cloud objects (Fig. 5). In the open ocean grids, histograms of these parameters are close to lognormal distributions with narrow peaks, typical of cumulus and stratocumulus types shown in Figs. 3 and 4. The peak powers at the modes increase as the grid moves further away from the coast. This indicates the transition from stratocumulus to cumulus types although purely exponential distributions for LWP and τ, typical of cumulus cloud objects, are not observed in either Grid 6 or 7. On the other hand, the contribution by stratocumulus type at Grid 1 is obvious, as evidenced by a two-mode distribution in TOA albedo and significant peaks at low liquid water path and τ. The droplet radius histograms can be divided into two groups, small droplet radius for the stratus-dominated regimes for Grids 1 and 2 and larger droplet radius for other five grids.

The stratus-to-cumulus transition across this Pacific transect is not dramatic in cloud macrophysical properties. However, the gradual shifts in the modes of the distributions in cloud-top temperature, OLR and cloud-top heights are readily seen from Figs. 11b, c and e. They are associated with the shifts in the SST distributions (Fig. 11a). The SST distributions are flat for Grids 1 and 2, which are associated with large seasonal variations of SST near the coast. The secondary modes in the OLR distribution are most likely associated with the cold SST and optically thick

clouds in these areas. In the other grids, there is only one mode in the OLR distributions. The shifts in the modes of OLR and cloud-top height follow those of SST. This is also partially resulted from the transition of cloud types because optically thin clouds are associated with higher OLR. The cloud-top height distribution is more complicated because it depends upon the proportion of different cloud object types in the grids. The lowest clouds occurred near the coast and near the equator. The lower coastal clouds are related to the lower PBL depths while the lower equatorial clouds are contributed by the cumulus cloud type (Fig. 3). The highest cloud tops occur in the middle of the transect, which are also associated with relatively low cloud-top temperatures and OLRs.

In summary, the relative population of the three cloud object types determines the overall cloud object physical properties in this Pacific transect because all cloud object types are combined into one population. This illustrates the importance of separating the boundary-layer clouds into physically distinct types, as done in sections 3-5. The relative frequency of occurrence for each cloud object type and each cloud object size, which is presumably linked to local dynamics, SST distribution and other factors, will then determine the overall cloud property distributions in a region.

7. Summary and discussion

Three boundary-layer cloud object types, stratus, stratocumulus and cumulus, occurred in the Pacific during January-August 1998, have been examined using the CERES SSF data from the TRMM satellite. This study has emphasized the contrasts and similarities in the characteristics of each cloud-object type between the tropical and subtropical regions and among different size categories and among small geographic areas, in relation to the physical processes that may cause differences among cloud object populations. Both the frequencies of occurrence and statistical distributions of cloud physical properties are analyzed for each of the three cloud object types.

For the frequencies of occurrence, stratocumulus clouds dominate the total boundary-layer cloud population in all regions and among all size categories. Stratus clouds are more prevalent in

the subtropics and near the coastal regions while cumulus clouds are relatively prevalent over open ocean and the equatorial regions, particularly the small size categories. The large-size stratus cloud objects with equivalent diameters greater than 300 km occur more frequently in the subtropics than in the tropics and have much larger average size than their cumulus and stratocumulus counterparts. The relative proportion is even more strongly impacted by large-scale circulations in smaller geographic regions than in the entire subtropical region of the Pacific Ocean.

Each of the three cloud object types exhibits small differences in statistical distributions of cloud optical depth and liquid water path, TOA albedo and perhaps cloud-top height, but large differences in those of cloud-top temperature and OLR between the tropics and subtropics. The latter two cloud physical properties are linked to the differences in the SST distributions between the tropics and subtropics. However, these differences between the tropics and subtropics are much smaller than those among the three cloud object types, which suggests that SST distributions influence some of the cloud macrophysical properties, but cloud microphysical properties and albedo for each cloud object type are determined by the (local) boundary-layer dynamics and structures.

There are significant dependencies of nearly all cloud object properties on their horizontal sizes. Systematic variations of cloud optical depth, TOA albedo, cloud-top height and OLR and SST with cloud object sizes are particularly pronounced for the stratocumulus and stratus types. This result can be explained by the systematic variations of large-scale dynamics with cloud object sizes, particularly, the strength of inversion produced by large-scale subsidence. Direct evidence from the matched European Center for Medium-range Weather Forecasts (ECMWF) soundings was not provided in this study because boundary-layer clouds were not well represented in the model during the data period. Comparisons of the surface divergences between ECMWF and QuikSCAT observations (Liu 2002) show large differences for cloud objects identified from the Terra satellite. The differences in cumulus cloud objects among the size categories are less systematic, due probably to weaker inversions associated with cumulus cloud objects and

larger uncertainties in the remotely sensed cloud parameters for broken clouds than for contiguous clouds.

The differences in cloud macrophysical properties over three small eastern Pacific regions are significantly larger than over the large tropical and subtropical Pacific regions. This result suggests a greater control of (local) large-scale dynamics and other factors on the cloud object properties because these factors vary more greatly from one area to another. However, the differences in the distributions of liquid water path, cloud optical depth and TOA albedo are also modulated by changes of the proportion of different size categories of cloud object type because the relative proportion of different size categories is less robust than in a larger region such as the entire subtropical Pacific.

The relative population among the three cloud object types determines the overall cloud object properties in the Pacific transect when all cloud object types are combined into one population. This has illustrated the importance of separating the boundary-layer clouds into physically distinct types, as in Part I. The relative frequency of occurrence for each cloud object type and each cloud object size category will then determine the overall cloud property distributions. Local dynamics and SST distributions are key parameters for determining the relative frequency.

Part I found that the proportion of different boundary-layer cloud types is changed as the large-scale circulations are changed from El Niño to La Niña conditions but some of statistical cloud properties do not change for a cloud object size category. This study has also found that there are systematic variations of cloud optical depth, TOA albedo, cloud-top height and OLR and SST with cloud object sizes, particularly, for the stratocumulus and stratus types. This suggests that the proportion of different size categories of a cloud object type is also an important factor in determining the overall cloud properties in a region. This proportion seems to change from one region to another due to differences in large-scale circulations and SST. Implication of this result is that the change in the frequency of occurrences among the size categories and its relationship with large-scale circulations are also important to determine the change in the overall cloud properties and cloud-radiative forcings. Bony and Dufresne (2005) suggested that a better understand-

ing of the behavior of boundary-layer clouds with changing environmental conditions will be critical to reduce the uncertainty in model predictions of tropical cloud feedbacks and climate sensitivity. This will require a much larger volume of cloud object information than presented in this study in order to increase the robustness of the estimated change in cloud properties with respect to atmospheric states.

These results are based upon eight months of the TRMM CERES data. It will be interesting to investigate these cloud object types using the Terra and Aqua CERES data, especially, their relationships with the matched atmospheric states. The cloud macrophysical properties of the Terra and Aqua CERES data are retrieved from higher-resolution imagers with smaller uncertainties than those of TRMM CERES data. The matched atmospheric states such as the surface divergence may be more reliable due to the assimilation of QuikSCAT surface wind data (Liu 2002) into meteorological model analyses for the recent data period. The effort of producing a large volume of cloud object data from the Terra and Aqua CERES data is underway and the new results will be reported in a separate study.

Acknowledgments: The CERES data were obtained from the Atmospheric Sciences Data Center at the NASA Langley Research Center. This research has been supported by NASA EOS interdisciplinary study program (Dr. Donald Anderson, Program Manager) and by the NSF grant ATM-0336762. The authors would also like to acknowledge Dr. Bruce Barkstrom of NOAA National Climatic Data Center and Professor David Randall of Colorado State University for their earlier insightful vision to this project.

References

Albrecht, B. A., D. A. Randall, and S. Nicholls, 1988: Observations of marine stratocumulus clouds during FIRE. *Bull. Amer. Meteor. Soc.,* **69,** 618-626.

Albrecht, B. A., C. S. Bretherton, D. Johnson, W. H. Schubert, and A. S. Frisch, 1995: The Atlantic Stratocumulus Transition Experiment -- ASTEX. *Bull. Amer. Meteor. Soc.,* **76,** 889-904.

Arawaka, A., 1975: Modeling clouds and cloud processes for use in climate models. *The Physical Basis of Climate and Climate Modeling.* GARP Publication Series No. 16, 183-197.

Barker, H. W. and B. A. Wielicki, 1997: Parameterizing grid-averaged longwave fluxes for inhomogeneous marine boundary layer clouds. *J. Atmos. Sci.*, **54**, 2785-2798.

Barker, H. W., B. A. Wielicki, and L. Parker, 1996: A parameterization for computing grid-averaged solar fluxes for inhomogeneous marine boundary layer clouds. Part II: Validation using satellite data. *J. Atmos. Sci.*, **53**, 2304-2316.

Bony, S., and J.-L. Dufresne, 2005: Marine boundary layer clouds at the heart of tropical cloud feedback uncertainties in climate models, *Geophys. Res. Lett.*, **32,** L20806, doi:10.1029/2005GL023851.

Bretherton, C. S., and coauthors, 2004: The EPIC 2001 stratocumulus study. *Bull. Amer. Meteor. Soc.,* **85,** 967-977.

Cess, R. D., M. Zhang, P.-H. Wang and B. A. Wielicki, 2001: Cloud structure anomalies over the tropical Pacific during the 1997/98 El Niño. *Geophys. Res. Lett.*, **28**, 4547-4550.

Dong, X., P. Minnis, G. G. Mace, W. L. Smith, Jr., M. Poellot, R. T. Marchand, and A. D. Rapp, 2002: Comparison of stratus cloud properties deduced from surface, GOES, and aircraft data during the March 2000 ARM cloud IOP. *J. Atmos. Sci.,* **23,** 3265-3284.

Efron, B. and Tibshirani, R., 1993: *An Introduction to the Bootstrap*. Chapman & Hall, 436 pp.

Garreaud, R. D., J. Rutllant, J. Quintana, J. Carrasco, and P. Minnis, 2001: CIMAR-5: A snapshot of the lower troposphere over the subtropical southeast Pacific. *Bull. Amer. Meteor. Soc.,* **82,** 2193-2207.

Greenwald, T. J., G. L. Stephens, S. A. Christopher, and T. H. Vonder Haar, 1995: Observations of the global characteristics and regional radiative effects of marine cloud liquid water. *J. Climate,* **8,** 2928-2946.

Hahn, C. J., W. B. Rossow, and S. G. Warren, 2001: ISCCP cloud properties associated with standard cloud types identified in individual surface observations. *J. Climate,* **14,** 11-28.

Jakob, C., G. Tselioudis, and T. Hume, 2005. The radiative, cloud and thermodynamic properties of the major Tropical Western Pacific cloud regimes. *J. Climate*, **18,** 1203-1215.

Klein, S. A., and D. L. Hartmann, 1993: The seasonal cycle of low stratiform clouds. *J. Climate,* **6,** 1587-1606.

Lau, N.-C., and M. W. Crane, 1995: A satellite view of the synoptic-scale organization of cloud properties in midlatitude and tropical circulation systems. *Mon. Wea. Rev.,* **123,** 1984-2006.

Lau, N.-C., and M. W. Crane, 1997: Comparing satellite and surface observations of cloud patterns in synoptic-scale circulation systems. *Mon. Wea. Rev.,* **125,** 3172-3189.

Loeb, N. G., S. Kato, K. Loukachine, N. Manalo-Smith, and D. R. Doelling, 2006a: Angular distribution models for top-of-atmosphere radiative flux estimation from the Clouds and the Earth's Radiant Energy System Instrument on the Terra satellite. Part II: Validation. *J. Atmos. Oceanic Tech.*, (in press)

Loeb, N. G., W. Sun, W. F. Miller, K. Loukachine, and R. Davies, 2006b: Fusion of CERES, MISR, and MODIS measurements for top-of-atmosphere radiative flux validation. *J. Geophys. Res.*, **111**, D18209, doi:10.1029/2006JD007146.

Liu, W. T., 2002: Progress in scatterometer application. *J. Oceanogr.,* **58,** 121-136.

Luo, Y., K.-M. Xu, B. A. Wielicki, T. Wong and Z. A. Eitzen, 2006: Statistical analyses of satellite cloud object data from CERES. Part III: Comparison with cloud-resolving model simula-

tions of tropical convective clouds. *J. Atmos. Sci.* (accepted). [Available from http://asd-www.larc.nasa.gov/~tak/wong/f23m.pdf]

Minnis, P.; D. Y. Young, D. P. Kratz; J. A. Coakley, Jr.; M. D. King, D. P. Garber, P. W. Heck, S. Mayor, and R. F. Arduini, 1997: Cloud Optical Property Retrieval (Subsystem 4.3). "Clouds and the Earth's Radiant Energy System (CERES) Algorithm Theoretical Basis Document, Volume III: Cloud Analyses and Radiance Inversions (Subsystem 4)," edited by CERES Science Team, December, 1997, 60 pp. [http://asd-www.larc.nasa.gov/ATBD/ATBD.html]

Randall, D. A., J. A. Coakley Jr., C. W. Fairall, R. A. Kropfli, and D. H. Lenschow, 1984: Outlook for research on subtropical marine stratiform clouds. *Bull. Amer. Meteor. Soc.,* **65,** 37-40.

Rossow, W. B., and R. A. Schiffer, 1991: ISCCP cloud data products. *Bull. Amer. Meteor. Soc.*, **72**, 2-20.

Rossow, W. B., and R. A. Schiffer, 1999: Advances in understanding clouds from ISCCP. *Bull. Amer. Meteor. Soc.*, **80**, 2261-2287.

Rossow, W. B., Y. Zhang, and J. Wang, 2005: A statistical model of cloud vertical structure based on reconciling cloud layer amounts inferred from satellites and radiosonde humidity profiles. *J. Climate,* **18,** 3587-3605.

Rossow, W. B., G. Tselioudis, A. Polak, and C. Jakob, 2005: Tropical climate described as a distribution of weather states indicated by distinct mesoscale cloud property mixtures. *Geophys. Res. Lett.*, **32,** L21821, doi:10.1029/2005GL024584.

Rozendaal, M. A., and W. B. Rossow, 2003: Characterizing some of the influences of the general circulation on subtropical marine boundary-layer clouds. *J. Atmos. Sci.,* **60,** 711-728.

Rozendaal, M. A., C. B. Leovy, and S. A. Klein, 1995: An observational study of diurnal variations of marine stratiform cloud. *J. Climate,* **8,** 1795-1809.

Schiffer, R. A., and W. B. Rossow, 1983: The International Satellite Cloud Climatology Project (ISCCP): The first project of the World Climate Research Programme. *Bull. Amer. Meteor. Soc.,* **64,** 779-784.

Schlesinger, M. E., 1985: Feedback analysis of results from energy balance and radiative-convective models. Projecting the Climatic Effects of Increasing Carbon Dioxide, M. C. MacCracken and F. M. Luther, Eds., U.S. Department of Energy, 280–319.

Siebesma, A. P., C. Jakob, G. Lenderink, R. A. J. Neggers, J. Teixeira, E. Van Meijgaard, J. Calvo, A. Chlond, H. Grenier, C. Jones, M. Köhler, H. Kitagawa, P. Marquet, A. P. Lock, F. Müller, D. Olmeda and C. Severijns, 2004: Cloud representation in general-circulation models over the northern Pacific Ocean: A EUROCS intercomparison study. *Quart. J. Roy. Meteor. Soc.,* **130,** 3245-3268.

Stevens, B., and coauthors, 2003: Dynamics and Chemistry of Marine Stratocumulus -- DYCOMS-II, 2003: *Bull. Amer. Meteor. Soc.*, **84,** 579-593.

Szczodrak, M., P. H. Austin, and P. B. Krummel, 2001: Variability of optical depth and effective radius in marine stratocumulus clouds. *J. Atmos. Sci.,* **58,** 2912-2926.

Tselioudis, G., and W. B. Rossow, 2006: Climate feedback implied by observed radiation and precipitation changes with midlatitude storm strength and frequency. *Geophy. Res. Lett.,* **33,** L02704, doi:10.1029/2005GL024513.

Tselioudis, G., Y. Zhang, and W. B. Rossow, 2000: Cloud and radiation variations associated with northern midlatitude low and high sea level pressure regimes. *J. Climate,* **13,** 312-327.

Weare, B. C., 2000: Near-global observations of low clouds. *J. Climate,* **13,** 1255-1268.

Wielicki, B. A., and Parker, L. 1992: On the determination of cloud cover from satellite sensors: The effect of sensor spatial resolution. *J. Geophys. Res.*, **97**, 12,799-12,823.

Wielicki, B. A., and R. M. Welch, 1986: Cumulus cloud properties derived using Landsat satellite data. *J. Clim. Appl. Meteor.,* **25,** 261-276.

Wielicki, B. A., R. D. Cess, M. D. King, D. A. Randall, and E. F. Harrison, 1995: Mission to Planet Earth: Role of clouds and radiation in climate. *Bull. Amer. Meteor. Soc.,* **76,** 2125-2153.

Wielicki, B. A., B. R. Barkstrom, E. F. Harrison, R. B. Lee III, G. L. Smith, and J. E. Cooper, 1996: Clouds and the Earth's Radiant Energy System (CERES): An Earth Observing System Experiment. *Bull. Amer. Meteor. Soc.*, 77, 853-868.

Wielicki, B. A., T. Wong, R. P. Allan, A. Slingo, J. T. Kiehl, B. J. Soden, C. T. Gordon, A. J. Miller, S.-K. Yang, D. A. Randall, F. Robertson, J. Susskind, and H. Jacobowitz, 2002: Evidence for large decadal variability in the tropical mean radiative energy budget. *Science*, **295**, 841-844.

Wood, R., and D. L. Hartmann, 2006: Spatial variability of liquid water path in marine low cloud: The importance of mesoscale cellular convection. *J. Climate,* **19,** 1748-1764.

Xu, K.-M., 2006: Using the bootstrap method for a statistical significance test of differences between histograms. *Mon. Wea. Rev.*, **134,** 1442-1453.

Xu, K.-M., T. Wong, B. A. Wielicki, L. Parker, and Z. A. Eitzen, 2005: Statistical analyses of satellite cloud object data from CERES. Part I: Methodology and preliminary results of 1998 El Niño/2000 La Niña. *J. Climate,* **18,** 2497-2514.

Xu, K.-M., T. Wong, B. A. Wielicki, L. Parker, B. Lin, Z. A. Eitzen, and M. Branson, 2006: Statistical analyses of satellite cloud object data from CERES. Part II: Tropical convective cloud objects during 1998 El Niño and evidence for supporting the fixed anvil temperature hypothesis. *J. Climate,* (accepted). [Available from http://asd-www.larc.nasa.gov/~tak/wong/f21m.pdf]

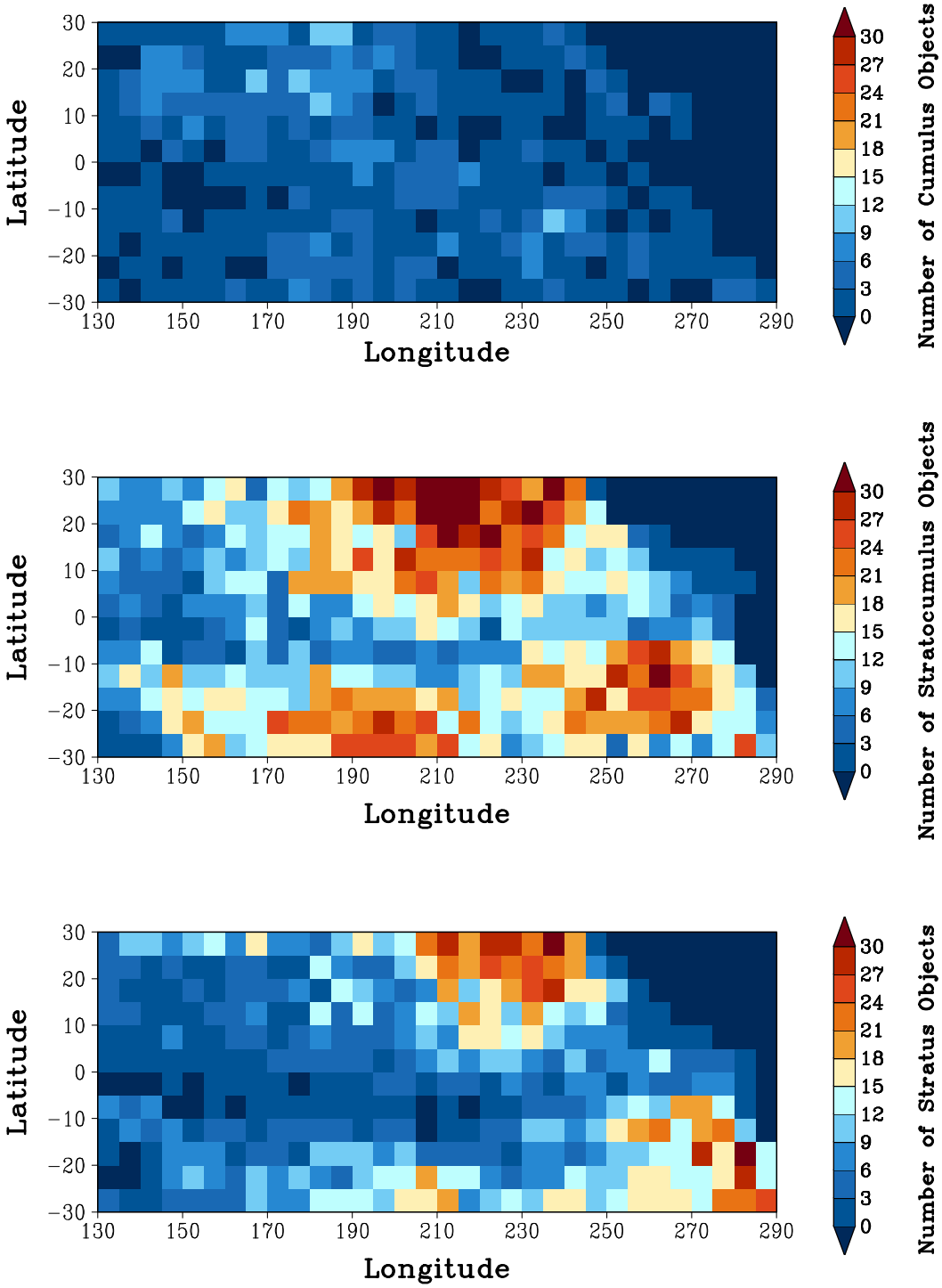

Figure 1: The accumulated number of cloud objects with equivalent diameters greater than 150 km observed during Jan-Aug 1998. The top panel is for the cumulus cloud objects, the middle the stratocumulus cloud objects and the bottom the solid stratus cloud objects.

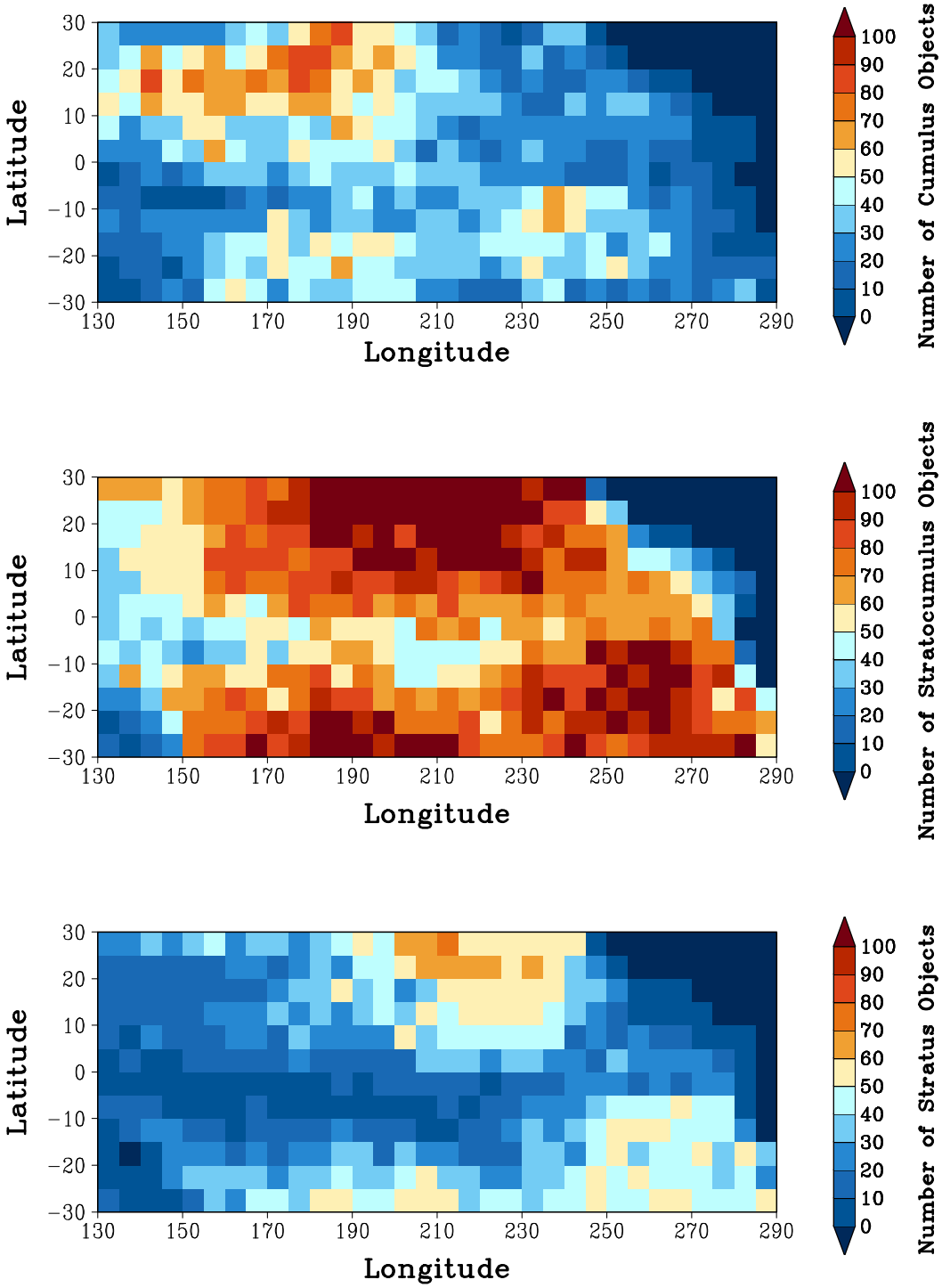

Figure 2: Same as Fig. 1 except for cloud objects with equivalent diameters greater than 75 km (including those large cloud objects shown in Fig. 1).

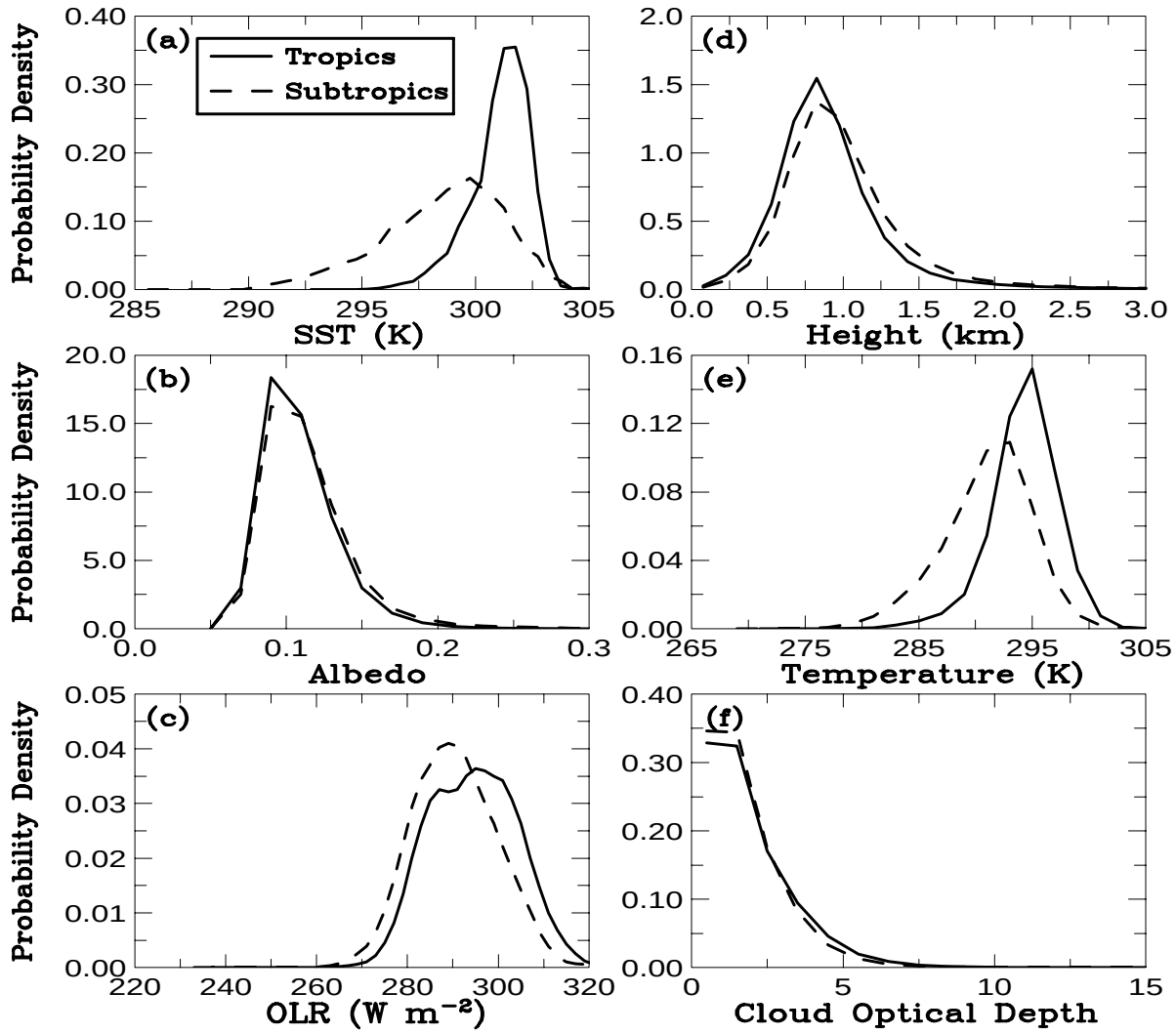

Figure 3: Summary histograms for (a) sea surface temperature, (b) top-of-the-atmosphere (TOA) albedo, (c) outgoing longwave radiation, (d) cloud-top height, (e) cloud-top temperature and (f) cloud optical depth of boundary-layer cumulus clouds objects in the tropics and subtropics for January-August 1998. All cloud objects with equivalent diameters between 75 and 300 km are included in the summary histograms.

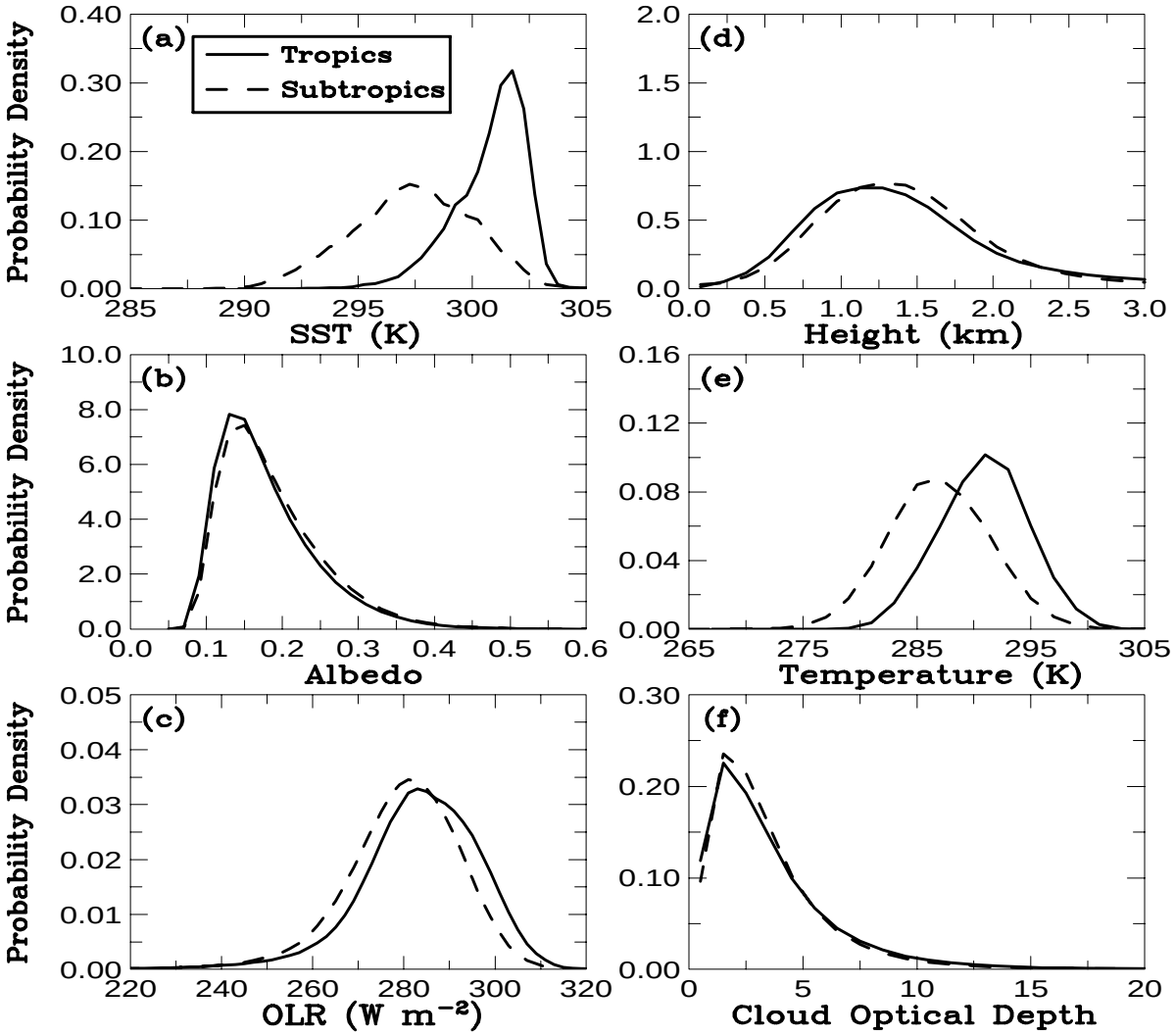

Figure 4: Same as Fig. 3 except for stratocumulus cloud objects.

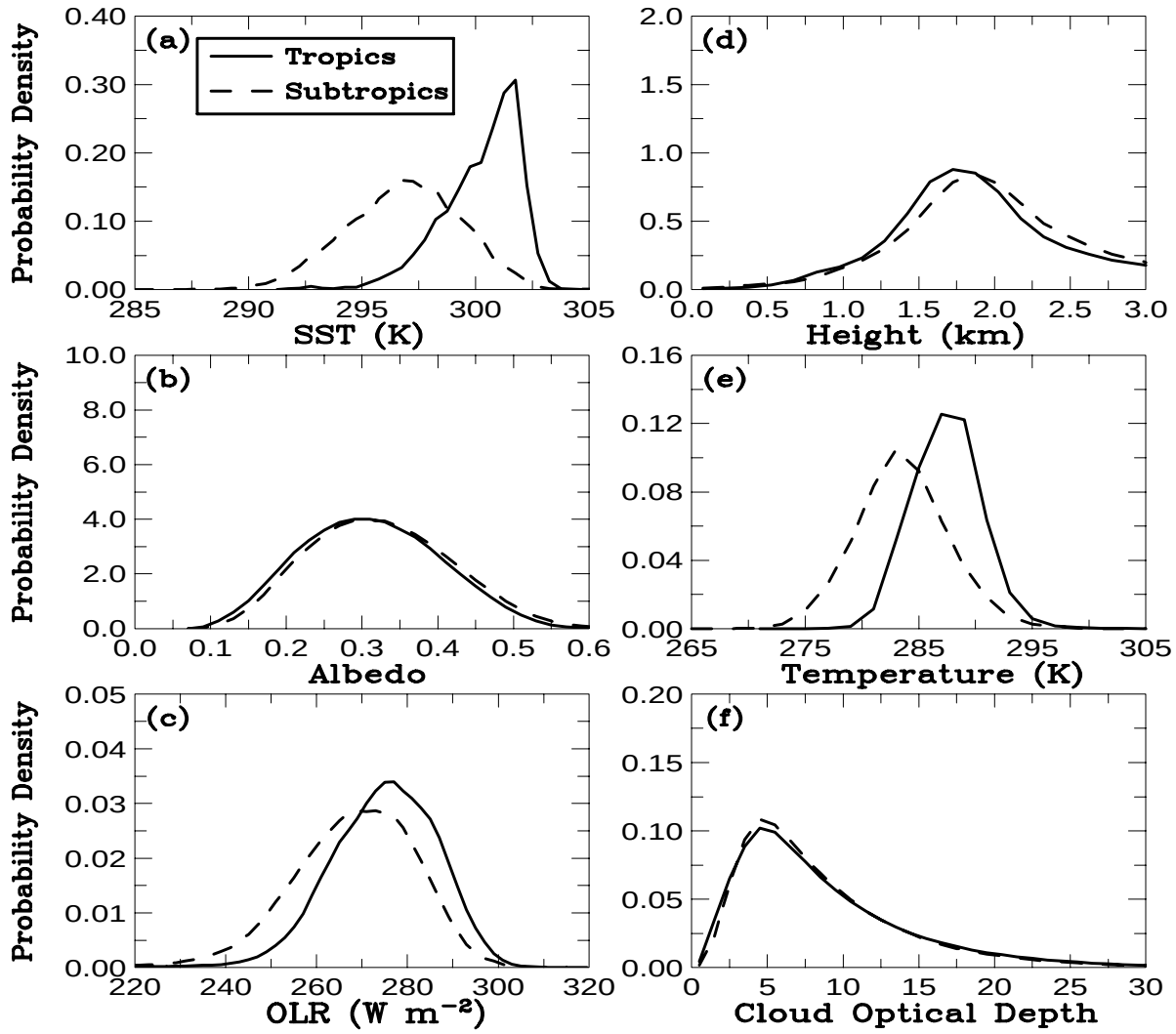

Figure 5: Same as Fig. 3 except for stratus cloud objects.

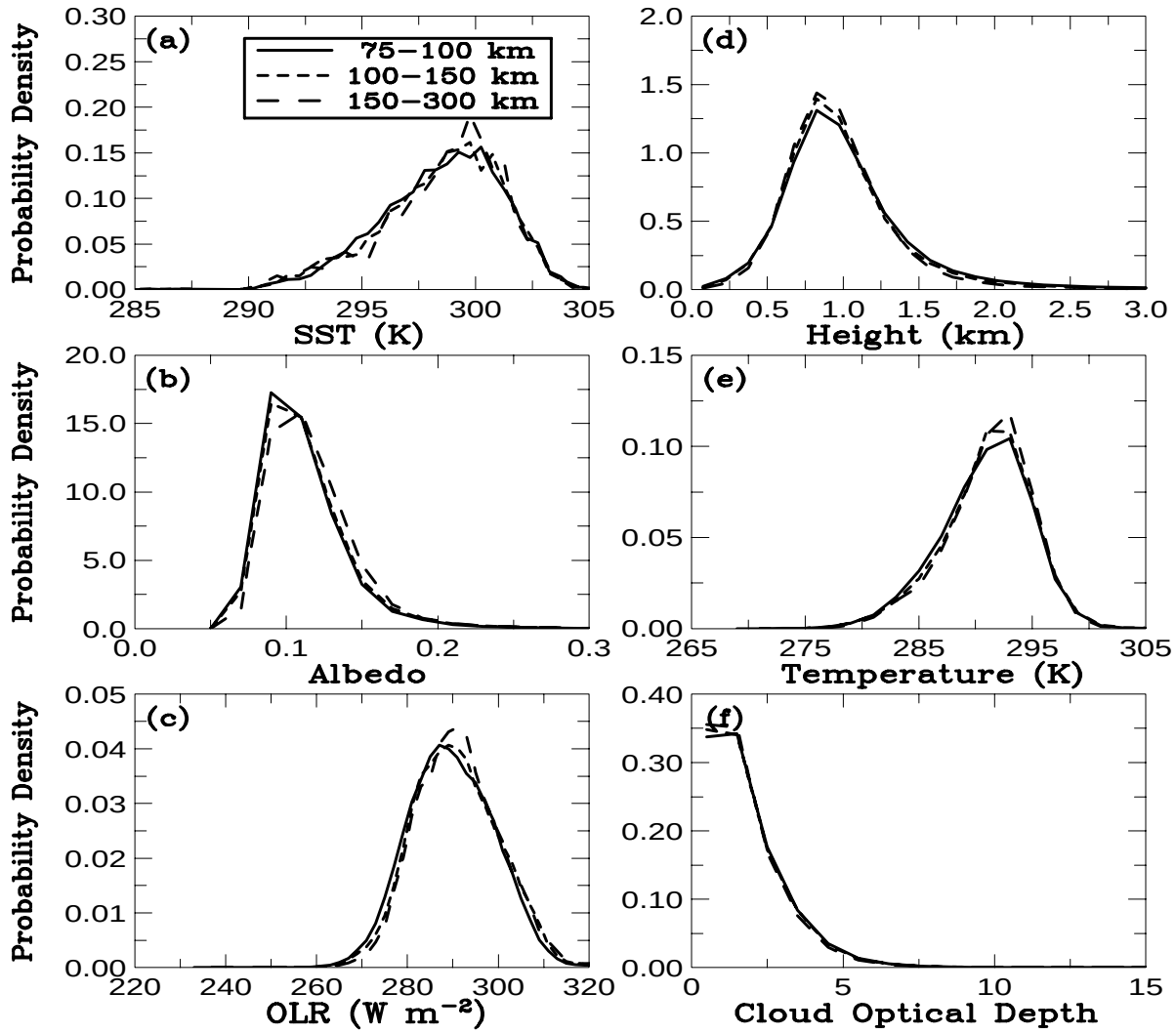

Figure 6: Same as Fig. 1 except for three size categories of subtropical cumulus cloud objects. The cloud objects in the three size categories have equivalent diameters of 75-100 km, 100-150 km and 150-300 km, respectively.

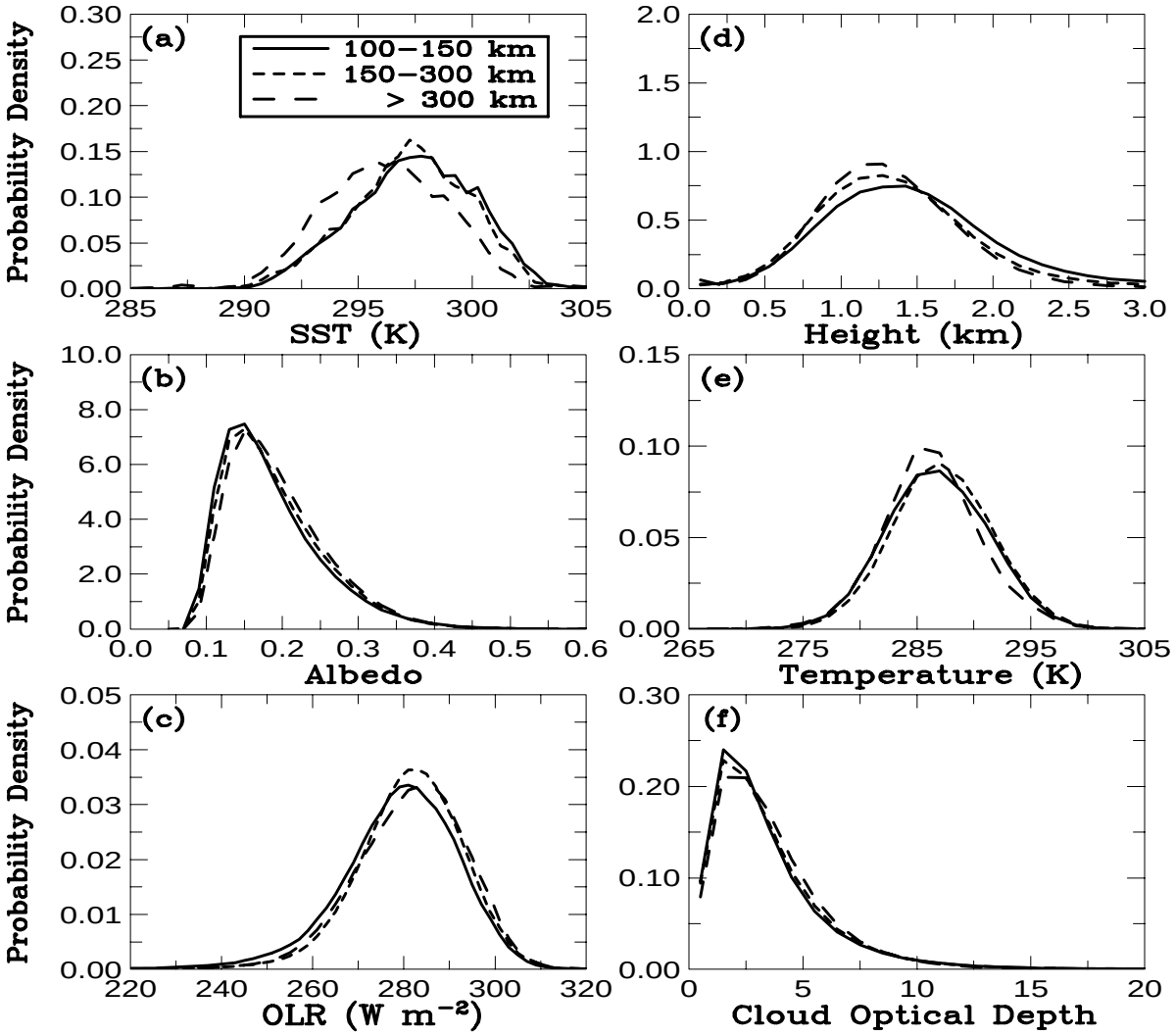

Figure 7: Same as Fig. 6 except for stratocumulus cloud objects with equivalent diameters of 100-150 km, 150-300 km and > 300 km, respectively.

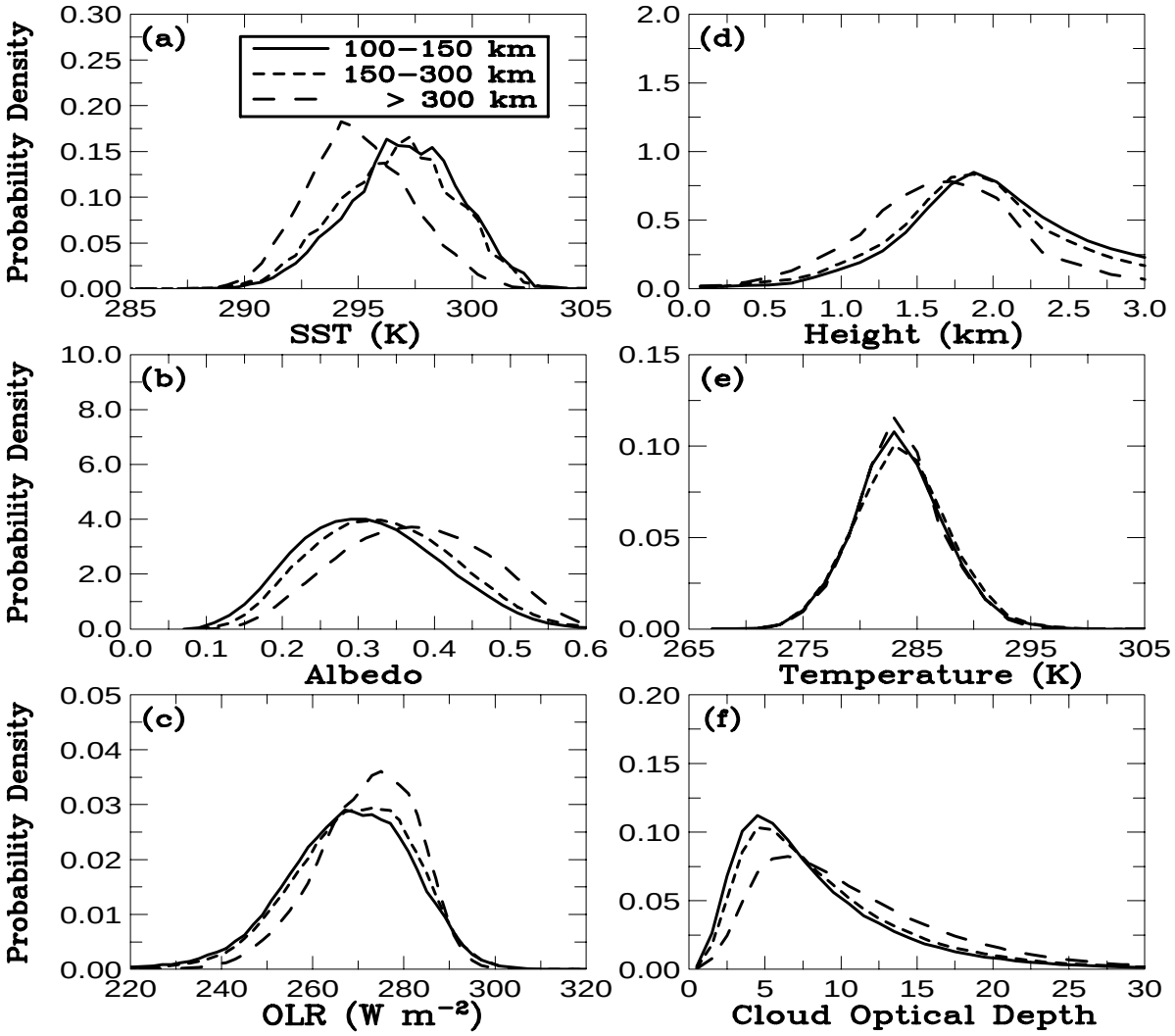

Figure 8: Same as Fig. 6 except for stratus cloud objects with equivalent diameters of 100-150 km, 150-300 km and > 300 km, respectively.

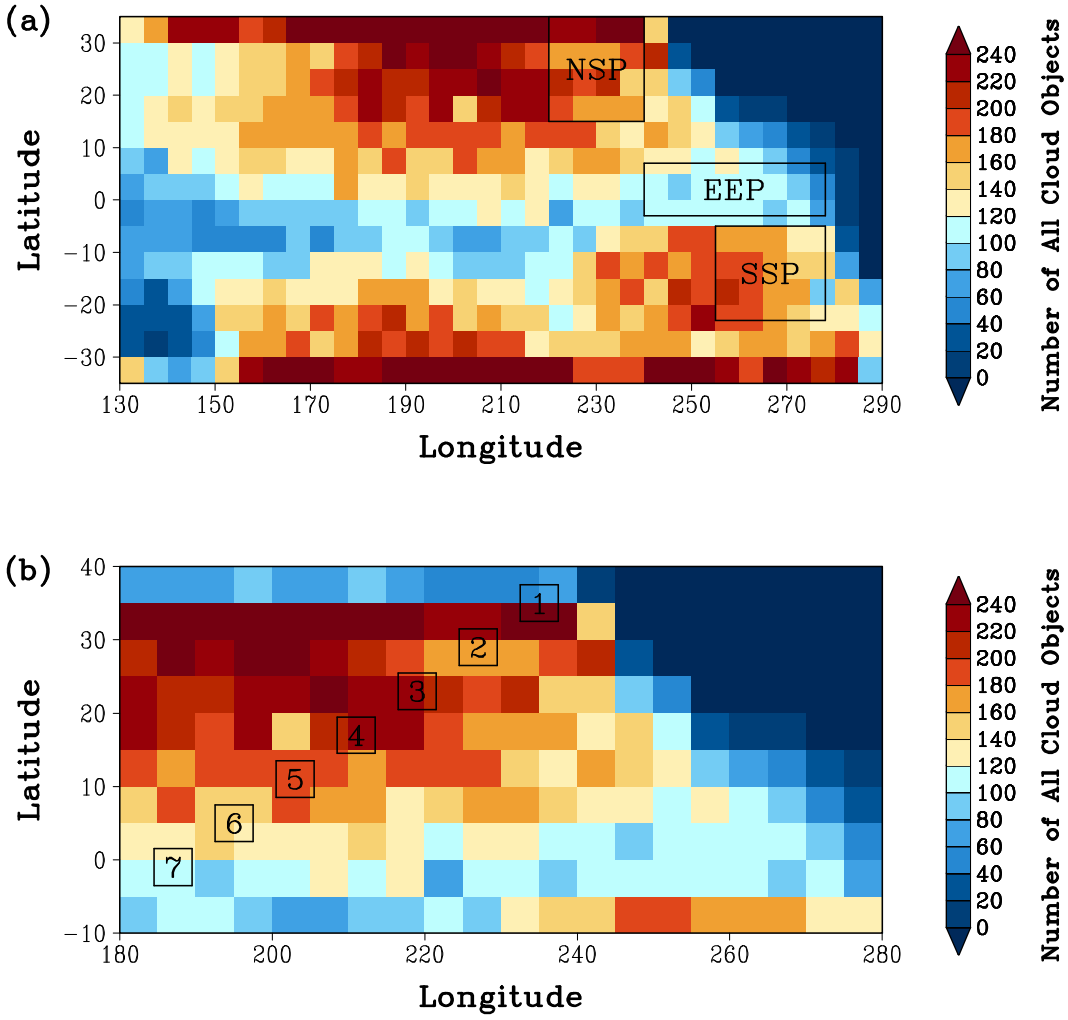

Figure 9: (a) Locations of three boundary-layer cloud dominating regions in the eastern Pacific and (b) the seven grids along a Pacific transect designed by the GCSS for a model intercompairson project. The accumulated number of three cloud object types with equivalent diameters greater than 75 km is also shown in both panels.

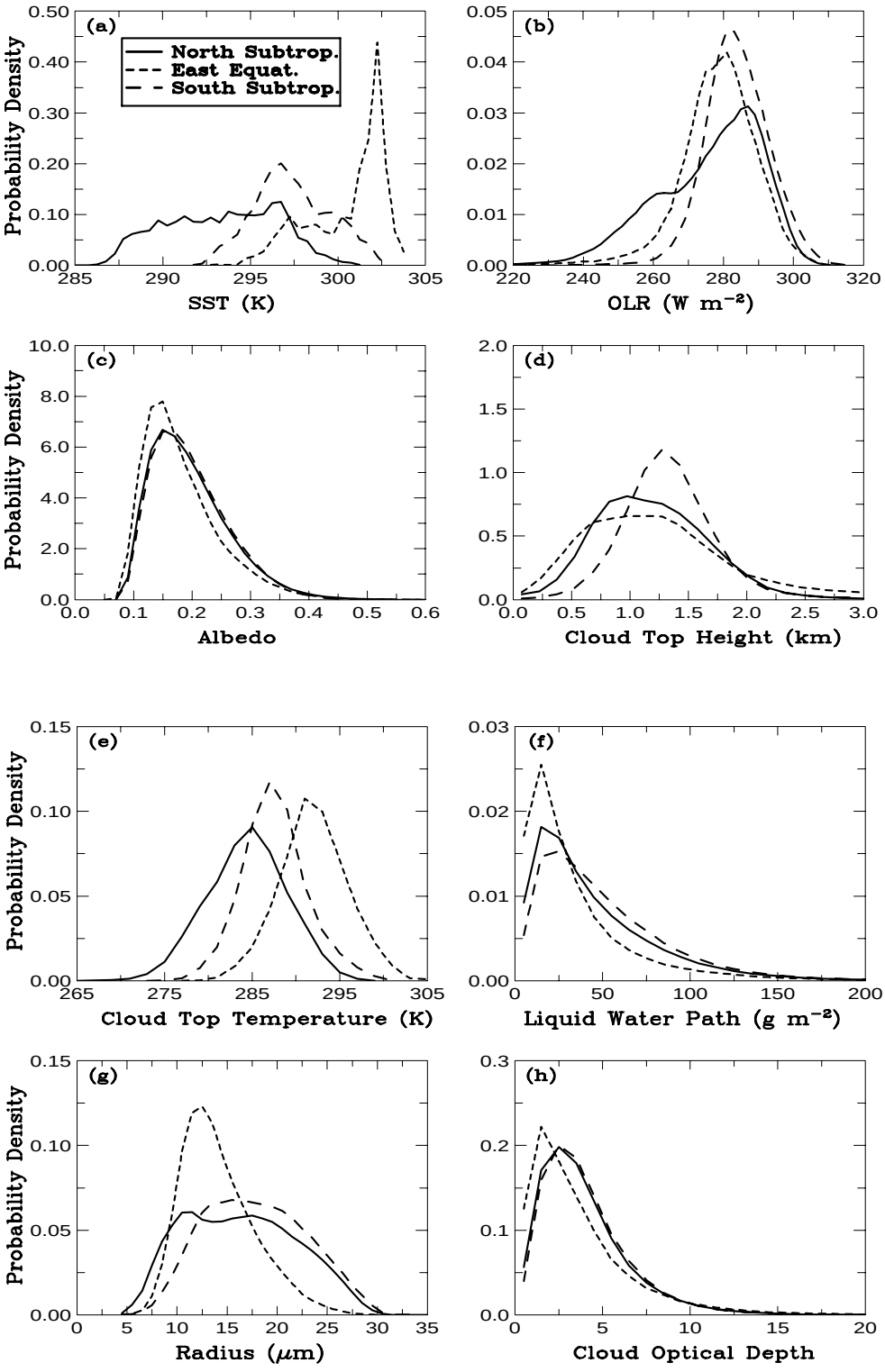

Figure 10: Same as Fig. 7 except for three stratocumulus dominated regions in the eastern Pacific. Two additional parameters (liquid water path and droplet radius) are also shown.

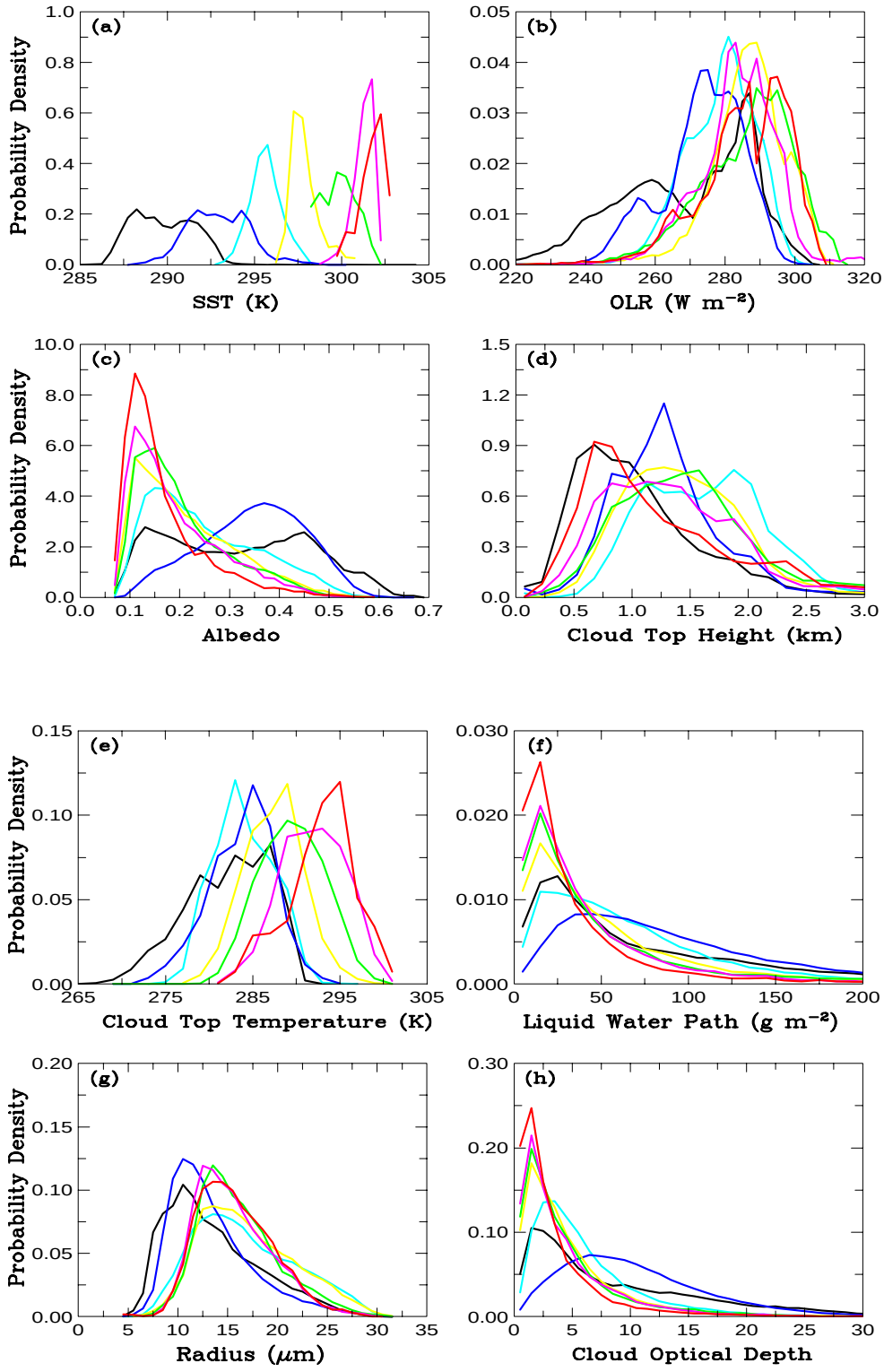

Figure 11: Same as Fig. 8 except for the GCSS Pacific transect and all cloud types combined. Grid numbers along the transit are indicated by black (Grid 1), blue (Grid 2), cyan (Grid 3), yellow (Grid 4), green (Grid 5), magenta (Grid 6) and red (Grid 7).

Table 1: A list of selection criteria for the boundary-layer cloud types.

Cloud object type	Cloud-top height	Cloud fraction	Latitude band
Cumulus	< 3 km	0.1 - 0.4	38 ° S - 38 ° N
Stratocumulus	< 3 km	0.4 - 0.99	38 ° S - 38 ° N
Stratus	< 3 km	0.99 - 1.0	38 ° S - 38 ° N

Table 2: The systematic biases and random errors in the measured footprint data of boundary-layer clouds and bin intervals of histogram used in this study.

Parameter	Systematic bias	Random error	Bin interval of histogram
OLR (W m^{-2})	< 0.5%	1-2%	4
TOA albedo	< 0.5%	2-3%	0.02
Cloud height (km)	0.2	0.3	0.15
Cloud temperature (K)	0.9	2.1	2.0
Liquid water path (g m^{-2})	-18	41	10.0
Droplet effective radius (μm)	0.7	1.8	1.0
Optical depth	-1.5	6.2	1.0

Table 3: Percent of the number of cloud-objects in the tropical and subtropical Pacific for four size categories of boundary-layer cumulus, stratocumulus and stratus cloud-object types during January-August 1998. The equivalent diameters of S1, S2, S3 and S4 size categories range from 75-100 km, 100-150 km, 150-300 km and > 300 km, respectively. The numbers of all-size (S1, S2, S3 and S4 combined) cloud objects are also shown in the table.

Cloud object type	Tropics					Subtropics				
	S1	S2	S3	S4	All sizes	S1	S2	S3	S4	All sizes
Cumulus	61.7	31.0	7.2	0.1	5,711	61.2	30.5	8.0	0.3	6,315
Stratocumulus	47.8	34.0	16.3	1.9	12,121	46.2	33.2	16.9	3.7	14,469
Stratus	40.5	32.6	21.3	5.6	4,025	38.0	30.5	20.2	11.3	6,139
All types	50.1	32.9	14.9	2.1	21,857	47.8	32.0	15.6	4.6	26,923

Table 4: Same as Table 3 except for the total footprint numbers, which are proportional to the total area coverages, for each size category in the tropical and subtropical regions. The total footprint numbers for all sizes are in thousand.

Cloud object type	Tropics					Subtropics				
	S1	S2	S3	S4	All sizes	S1	S2	S3	S4	All sizes
Cumulus	38.8	37.6	22.0	1.6	500.2	37.1	35.6	24.4	2.9	576.8
Stratocumulus	19.7	27.6	36.4	16.3	1640.4	15.4	21.7	30.6	32.3	2435.3
Stratus	11.0	17.5	34.4	37.1	830.3	5.5	8.8	17.3	68.4	2379.0
All types	20.5	26.4	33.4	19.7	2970.9	13.3	17.5	24.1	45.1	5391.1

Table 5: Statistics of the footprint numbers for the S4 size categories of boundary-layer cloud object types in the tropical and subtropical regions.

Cloud object type	Region	Mean	Median	Standard deviation	Minimum	Maximum
Stratocumulus	Tropics	1145	953	569	685	4579
	Subtropics	1459	1132	867	683	5679
Stratus	Tropics	1369	1035	1042	686	7384
	Subtropics	2350	1480	2132	684	15125

Table 6: The statistical significance levels or *p* values between a pair of size categories for different parameters of the three subtropical boundary-layer cloud object types. See text for the definition of size categories S1, S2, S3 and S4 and the explanation of p values.

Parameter	Cumulus			Stratocumulus			Stratus		
	S1, S2	S2, S3	S1, S3	S2, S3	S3, S4	S2, S4	S2, S3	S3, S4	S2, S4
SST	0.49	0.78	0.39	0.44	< 0.01	< 0.01	0.13	< 0.01	< 0.01
OLR	0.22	0.74	0.08	< 0.01	0.06	< 0.01	0.14	< 0.01	< 0.01
Albedo	0.29	< 0.01	< 0.01	< 0.01	< 0.01	< 0.01	< 0.01	< 0.01	< 0.01
Cloud height	0.01	0.19	< 0.01	< 0.01	< 0.01	< 0.01	< 0.01	< 0.01	< 0.01
Cloud temperature	0.04	0.31	0.01	< 0.01	< 0.01	< 0.01	0.09	0.04	0.55
LWP	0.97	0.65	0.70	< 0.01	< 0.01	< 0.01	0.01	0.17	< 0.01
Droplet radius	0.06	0.07	< 0.01	< 0.01	< 0.01	< 0.01	0.04	< 0.01	< 0.01
Optical depth	0.39	0.41	0.11	< 0.01	< 0.01	< 0.01	< 0.01	< 0.01	< 0.01

Table 7: Number of boundary-layer cloud objects for the S2, S3 and S4 size categories and their sum in three eastern Pacific regions. See text for the definition of these regions.

Cloud object type	Southern Subtropics				Eastern Equatorial				Northern Subtropics			
	S2	S3	S4	Sum	S2	S3	S4	Sum	S2	S3	S4	Sum
Cumulus	115	25	1	141	66	8	0	74	104	30	1	135
Stratocumulus	505	299	94	898	332	139	6	477	583	363	111	1057
Stratus	218	187	104	509	111	88	20	219	261	195	255	711
All types	838	511	199	1548	509	235	26	770	948	588	367	1903

Table 8: Same as Table 7 except for the Pacific transect. The accumulated number of S2, S3 and S4 size cloud objects whose centers are located within each of seven 5° x5° grids is shown. Grid 1 is closest to the California coast and Grid 7 to the Equator (see Fig. 9b). The total footprint number is shown at the bottom row.

	Grid 1	Grid 2	Grid 3	Grid 4	Grid 5	Grid 6	Grid 7
Cumulus	22	3	8	18	17	16	15
Stratocumulus	91	63	72	71	67	38	29
Stratus	38	45	44	29	28	13	5
Total	151	111	124	118	112	67	49
Total footprint	70,760	126,113	40,197	27,532	20,964	15,516	8,666